iScience

CellPress
OPEN ACCESS

Article

Role of caveolin-1 in metabolic programming of fetal brain

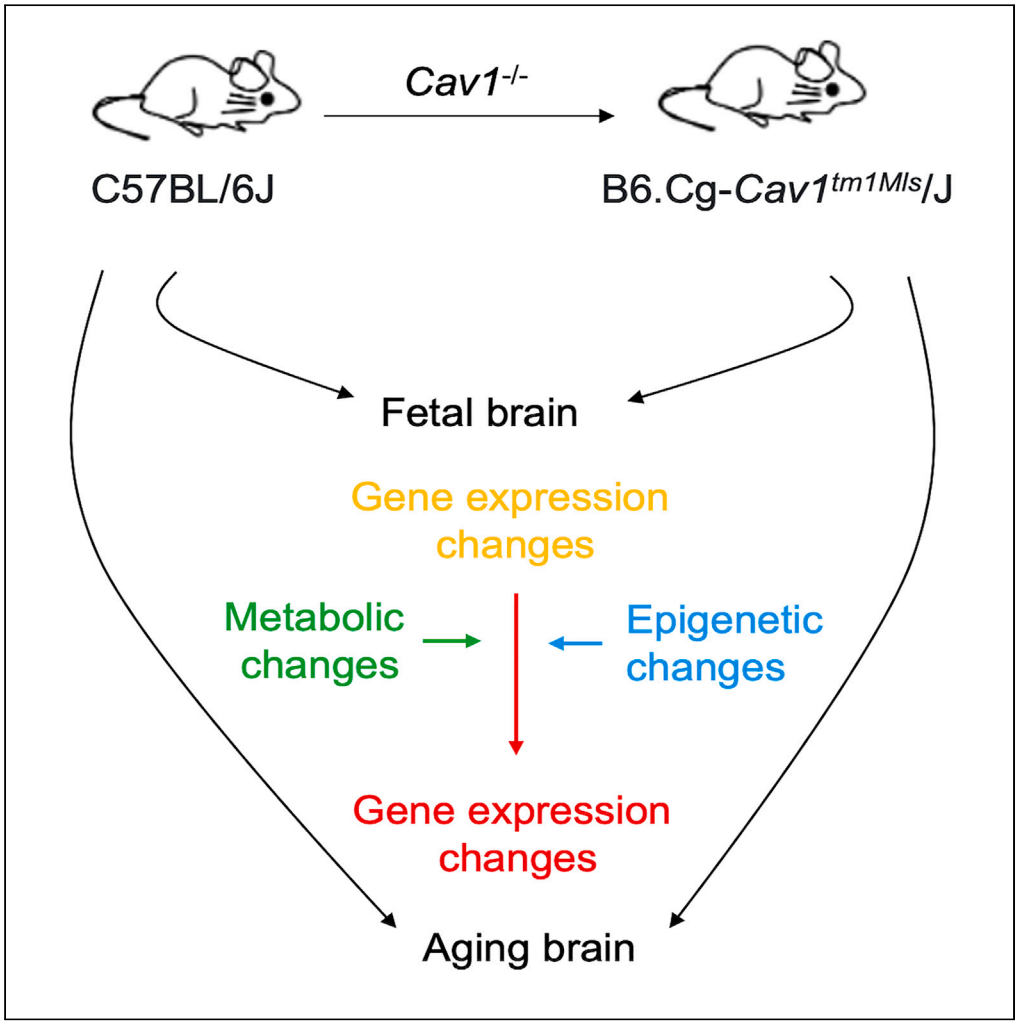

Maliha Islam,
Susanta K. Behura

behuras@missouri.edu

Highlights

Ablation of *Cav1* deregulates fetal brain metabolism

Loss of *Cav1* alters DNA methylation of metabolic genes in fetal brain

Specific cell types of fetal brain are impacted due to the loss of *Cav1*

Lack of *Cav1* affects gene expression of the brain upon aging

Islam & Behura, iScience *26*, 107710
October 20, 2023
https://doi.org/10.1016/j.isci.2023.107710

iScience

CellPress
OPEN ACCESS

Article

Role of caveolin-1 in metabolic programming of fetal brain

Maliha Islam[1] and Susanta K. Behura[1,2,3,4,5,*]

SUMMARY

Mice lacking caveolin-1 (*Cav1*), a key protein of plasma membrane, exhibit brain aging at an early adult stage. Here, integrative analyses of metabolomics, transcriptomics, epigenetics, and single-cell data were performed to test the hypothesis that metabolic deregulation of fetal brain due to the ablation of *Cav1* is linked to brain aging in these mice. The results of this study show that lack of *Cav1* caused deregulation in the lipid and amino acid metabolism in the fetal brain, and genes associated with these deregulated metabolites were significantly altered in the brain upon aging. Moreover, ablation of *Cav1* deregulated several metabolic genes in specific cell types of the fetal brain and impacted DNA methylation of those genes in coordination with mouse epigenetic clock. The findings of this study suggest that the aging program of brain is confounded by metabolic abnormalities in the fetal stage due to the absence of *Cav1*.

INTRODUCTION

Development of the central nervous system (CNS) is a highly coordinated spatiotemporal process. It includes proliferation of glia and neurons and their migration, followed by programmed cell death, formation of synapses, myelination, and establishment of neuronal circuits. In mice, the development of the neural tube begins at gestation day 9–9.5.[1] Neurogenesis in the fetal brain increases with gestation whereas microglia, brain macrophages that function as the immune system of CNS, colonize in two phases during the mid and late gestational stages.[2] In contrast to microglia, synaptogenesis occurs during late gestation and then after birth.[3] Similarly, formation of the vascular network and angiogenesis begin early in CNS development while the genesis of astrocytes begins late in gestation around day 18.[3] On gestation day (GD) 15 when the placenta is fully functional,[4] extensive changes occur in the fetal brain that include formation of distinct layers of the cerebral cortex, development of GABAergic inhibitory neurons, formation of the pituitary stalk, and accelerated growth of neuronal population in the hindbrain. Generation of oligodendrocytes, pruning, and myelination predominantly occur during early postnatal periods.[3]

Our recent work showed that epigenetic aging of the mouse brain is programmed at the fetal stage.[5] In an earlier study, we also observed that sirtuin 6 (*Sirt6*) which regulates mouse longevity was expressed in the fetal brain in correlation with caveolin-1 (*Cav1*).[6] *Cav1* codes for a major membrane protein which is abundantly found in endothelial cells[7,8] and also in many other cell types with relatively lower abundance.[9–12] Mice lacking *Cav1* are viable and fertile but show phenotypes including impaired endothelial functions, angiogenesis, hyperproliferative and vascular abnormalities.[13] These mice show reduced lifespan[14] and exhibit neuronal aging at a young age (3–6 month old) that resembles the brain of one- and a half-year-old wild-type (WT) mice.[15] Multiple hallmarks of Alzheimer's disease (AD) such as increased amyloid beta, tau, astrogliosis, and shrinkage of cerebrovascular volume were observed in these mice at early adult age.[15] As *Cav1* influences beta-secretase which plays a key role in the production of amyloid beta peptides in AD brain,[16] links of *Cav1* have been suggested with AD symptoms in these mice.[15] Experiments with animal models of AD have shown that amyloid beta levels and gradual decline in cognitive ability are associated with abnormal conditions of the brain during early development.[17–20] The "*Latent Early life Associated Regulation*" (LEARn) model proposed by Lahiri and Maloney[21] suggests that changes in the epigenetic state of the brain during early life serve as precursors for development of AD pathologies later in life.

In the WT mouse fetal brain, *Cav1* plays a role in the clathrin-independent endocytosis to promote neuronal maturation.[10] As there are no caveolae in neuronal cells, *Cav1* functions in a caveolae-independent manner in neuronal cells.[10,22–24] Besides the role of *Cav1* in neuronal maturation, *Cav1* functions as a major regulator of cellular metabolism.[25–28] It plays important roles in the regulation of urea[29] and serine[16] as well as maintaining cellular homeostasis of cholesterol.[25] Loss of *Cav1* deregulates cholesterol metabolism in embryonic fibroblasts and peritoneal macrophages in mice.[13] Accumulating evidence suggests that specific stress or nutritional and/or metabolic abnormalities during fetal stages are linked to an increased risk of neurological disorders in adult life.[17,20,30–34] Studies have also shown that metabolic abnormalities in early life are linked to fetal epigenetic programming for adult health and diseases.[35–39] In addition, evidence suggests that epigenetic

[1]Division of Animal Sciences, 920 East Campus Drive, University of Missouri, Columbia, MO 65211, USA
[2]MU Institute for Data Science and Informatics, University of Missouri, Columbia, MO, USA
[3]Interdisciplinary Reproduction and Health Group, University of Missouri, Columbia, MO, USA
[4]Interdisciplinary Neuroscience Program, University of Missouri, Columbia, MO, USA
[5]Lead contact
*Correspondence: behuras@missouri.edu
https://doi.org/10.1016/j.isci.2023.107710

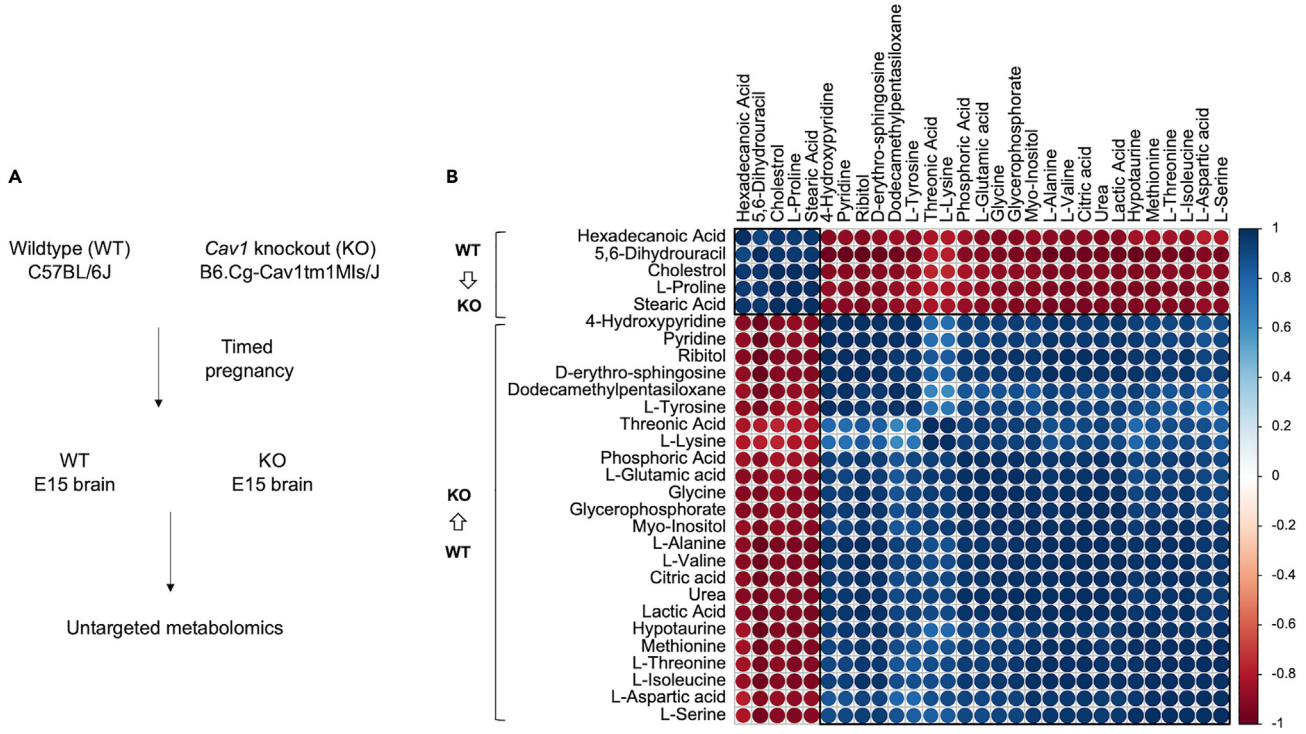

Figure 1. Experimental design and metabolomics analysis

(A) Timed pregnancy was performed separately with WT and *Cav1*-null mice to collect GD15 fetal brain. (B) Pairwise cluster analysis of variation of metabolite levels show that specific lipids, including cholesterol, were suppressed whereas several amino acids were activated in the fetal brain due to the absence of *Cav1*.

memory plays a key role to control the effects of early life environmental stresses on development, aging, and passing on parental exposures and experiences to offspring.[39–42] Epigenetic memory is an emerging concept in fetal origin of adult health and disease.[39,43–45] As *Cav1*-null mice show abnormal metabolism compared to WT mice,[13,46–48] it is significant to understand how the loss of *Cav1* influences brain development and aging in mice.

The purpose of this study is to investigate metabolic, epigenetic, and transcriptomic change of mouse fetal brain due to the ablation of *Cav1*. A particular aim is to identify metabolism genes that are altered in the fetal brain at the transcriptional and epigenetic levels due to the loss of *Cav1*. In addition, this study aims to identify genes that are altered in the brain, both at fetal and aging stages, of *Cav1*-null compared to WT mice. The final aim of this study is to identify cell types of the fetal brain and investigate expression of the impacted metabolism genes in the individual cell types of the fetal brain in a comparative manner in *Cav1*-null compared to WT mice.

RESULTS

Metabolic deregulation of fetal brain due to Cav1 ablation

We performed untargeted metabolomics analysis of GD15 fetal brain, representing both sexes of WT and *Cav1*-null mice, to identify metabolites that were impacted due to the ablation of *Cav1*. A total of 139 and 142 metabolites were detected in the WT and *Cav1*-null fetal brain, respectively (Table S1). Of the 139 detected metabolites of the WT brain, the identity of 85 was known and that of the other 54 metabolites were unknown. In the *Cav1*-null brain, 81 were identified and the other 61 were unknown. While several metabolites showed female-bias expression in the WT mice, an opposite pattern was observed in *Cav1*-null mice (see Table S1). Though sex differences in the rate of metabolism are known in human,[49] this finding suggested that *Cav1* may play a role in brain metabolism in a sex-dependent manner. Specific lipids and amino acids were significantly ($p < 0.02$) deregulated in the fetal brain due to the loss of *Cav1* (Table S2). Cholesterol, hexadecanoic acid (also known as palmitic acid), and stearic acid decreased in the fetal brain of *Cav1*-null mice (Figure 1). While cholesterol and palmitic acid decreased by 10 and 4.7-folds, respectively, stearic acid decreased by ~100-folds. L-proline and 5,6-dihydrouracil also decreased significantly due to the absence of *Cav1* (Table S2). On the other hand, several amino acids and organic compounds significantly increased in the fetal brain in response to the loss of *Cav1*. The alpha glycerophosphate ester, an esterified form of glycerol, increased by ~60-fold. Among all the identified metabolites, urea was the most altered brain metabolite in the *Cav1*-null mice. Urea level increased drastically, by 2,183-folds, in the fetal brain of *Cav1*-null compared to WT mice suggesting a major role of *Cav1* in the regulation of brain urea.

By mapping the deregulated metabolites to the compounds database of Kyoto Encyclopedia of Genes and Genomes (KEGG), we further identified that these metabolites were associated with specific metabolic pathways (Table S2). The deregulated lipids were associated with

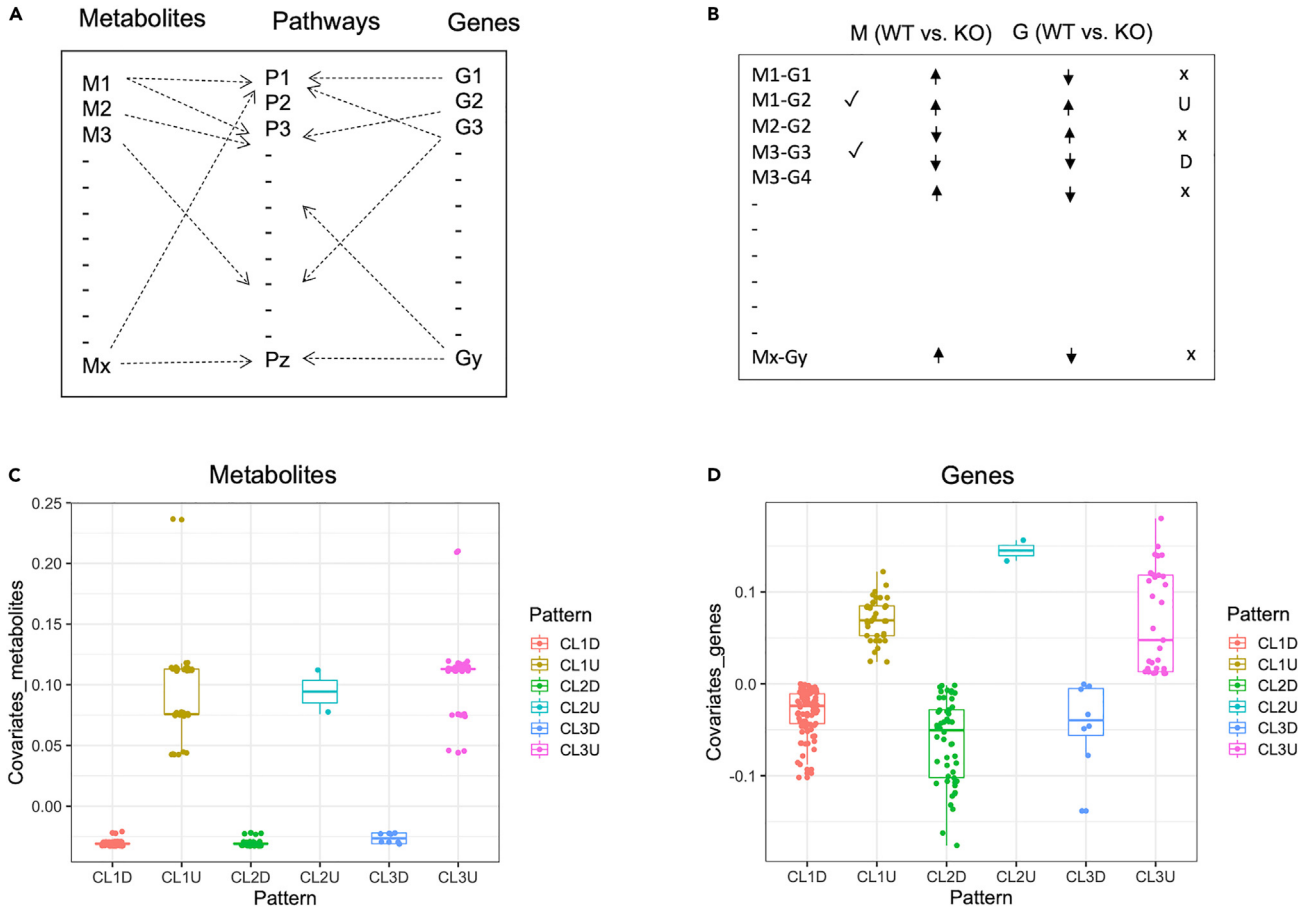

Figure 2. Integrative analysis of metabolomics and RNA-seq data

(A) Metabolites (Ms) were mapped to KEGG compounds database, and genes (Gs) were mapped to KEGG genes database to identify metabolite-gene pairs that mapped to the same pathways (Ps).

(B) The direction of change of metabolite and gene was then evaluated. Pairs in which both the gene and metabolite showed similar change (U: upregulation, D: downregulation) in the brain of *Cav1*-null compared to WT mice were extracted. They were subjected to canonical correlation analysis.

(C) Canonical changes of metabolites (U: upregulated, D: downregulated) clustered into three distinct clusters (CL1, CL2, and CL3). Each dot here represents a metabolite. The patterns of variation are shown in boxplots with different colors.

(D) Canonical changes of genes (U: upregulated, D: downregulated) in the same three clusters (CL1, CL2, and CL3). Each dot represents a gene. The patterns of variation are shown in boxplots with different colors.

cholesterol metabolism, bile acid and steroid hormone biosynthesis whereas the deregulated amino acids were associated with pathways of alanine, aspartate, and glutamate metabolism, GABA (gamma-aminobutyrate) shunt, histidine degradation, and arginine and proline biosynthesis.

Transcriptomic and epigenetic changes of metabolism genes in the fetal brain due to Cav1 ablation

RNA-seq was performed with the fetal brain (GD15) of WT and *Cav1*-null mice to investigate expression of metabolic pathway genes associated with the deregulated metabolites. RNA-seq data (accession numbers GEO: GSE215138 and GEO: GSE215139) analysis identified significant (false discovery rate <0.05) differential expression (DE) of 2,218 genes in the fetal brain of *Cav1*-null compared to that of the WT mice (Table S3). By mapping the deregulated genes and metabolites to KEGG databases, we identified metabolite-gene pairs that are associated with common KEGG pathways (Figure 2A). In the next step, we identified the pairs where both the metabolite and gene were either up regulated or downregulated due to the loss of *Cav1* (Figure 2B). The list of these co-regulated gene-metabolite pairs is listed in Table S4. Bicluster analysis[50] showed three distinct clusters (CL1, CL2, and CL3) in which these metabolites and genes varied in a canonical correlation[51] manner in *Cav1*-null compared to WT brain (Figures 2C and 2D). Enrichment analysis by hypergeometric test showed that specific metabolic pathways were significantly ($p < 0.05$) enriched by these co-regulated genes (Table 1). They are related to metabolism of starch and sugar, vitamins, sphingolipids, and amino acids. The covariate estimates of gene expression and metabolite changes in each cluster, based on canonical correlation analysis,[52] are listed in Table S5. Both CL1 and CL2 represented genes and metabolites associated with different lipid metabolism

Table 1. List of metabolic pathways significantly enriched by the metabolic genes differentially expressed in fetal brain of *Cav1*-null compared to WT mice

Pathway name	Pathway ID	p value	Fold enrichment
Starch and sucrose metabolism	mmu00500	0.009221	34
Retinol metabolism	mmu00830	0.000006	32.33
Sphingolipid metabolism	mmu00600	0.001619	27
Cysteine and methionine metabolism	mmu00270	0.001619	27
Amino sugar and nucleotide sugar metabolism	mmu00520	0.002664	25.5
Linoleic acid metabolism	mmu00591	0.003141	25
Porphyrin metabolism	mmu00860	0.009749	21.5
Nicotinate and nicotinamide metabolism	mmu00760	0.013375	20.5
Alanine, aspartate and glutamate metabolism	mmu00250	0.018279	19.5
Drug metabolism - other enzymes	mmu00983	0.000327	18.4
Arachidonic acid metabolism	mmu00590	0.002566	14.33
Purine metabolism	mmu00230	0.000329	13.4

pathways. However, we observed genes (*Dgkb*, *Pla2g4b*, *Prkcg*, *Coq3*, *Gng10*, *Gng11*, *Gng5*, *Prkcg* and *Prlr*, and *Ggh*) and metabolites (alpha-glycerophosphate ester, L-tyrosine, and methionine) that were expressed in CL1 but not in CL2. On the other hand, CL3 primarily represented amino acid metabolism pathway genes. Based on mutual information network analysis[53] and network centrality test,[54] specific metabolites and genes played central roles in the regulation of these pathways. *Aqp1* and *Adcy3*, and cholesterol were predicted as key gene-metabolite interactions in CL1 and CL2. *Dnah2* and glutamic acid were predicted as key gene-metabolite interaction in CL3. Mapping the genes associated with the clusters to known ligand-receptor genes,[55] we further identified specific ligand and receptor genes that were predominantly associated with cholesterol (Table S6). While our earlier study had identified a plethora of co-expressed ligand-receptor genes in the WT mouse fetal brain,[56] the current finding suggested that the loss of *Cav1* perturbated several receptor-ligand interactions due to the deregulation of cholesterol in the brain. A majority of these receptor-ligand genes were downregulated in the fetal brain of *Cav1*-null compared to that of WT mice supporting the idea that these genes are associated with the deregulation of cholesterol homeostasis in *Cav1*-null mice.[13] Besides cholesterol, we also observed ligand-receptor genes associated with D-*erythro*-sphingosine and L-glutamic acid (Table S6). The ligand and receptor genes associated with cholesterol altered in the same direction but those associated with D-*erythro*-sphingosine or L-glutamic acid altered in an opposite direction suggesting differential receptor-ligand signaling in the brain in response to *Cav1* ablation.

The RNA-seq data identified several DE genes that were associated with mouse epigenetic clock.[57] By profiling the methylation level of CpG (cytosine-guanine) associated with an epigenetic clock in the fetal brain of WT and *Cav1*-null mice (Table S7), we identified sites (n = 784) that were methylated at a higher level in the fetal brain of *Cav1*-null compared to WT mice (Figure 3). A lesser number of CpGs (n = 492) showed an opposite pattern of methylation. The Venn diagrams in Figure 3 show patterns of hyper and hypo-methylations (shown as "m") within the epigenetic clock genes (shown as "g") in the fetal brain of *Cav1*-null compared to WT mice. A total of 80 clock genes were hypo-methylated at 406 CpG sites, and another group of 63 clock genes were hyper-methylated at 232 sites in the *Cav1*-null brain compared to that of the WT brain. In addition, we identified a total of 60 genes each of which showed both the types of methylations. A total of 169 hypo-methylated and 133 hyper-methylated sites were identified in these genes. Specific metabolic genes were among these epigenetically altered gene groups. *Stard3*, *Dapk1*, *Bdnf*, and *Cpt1c* were hyper-methylated whereas *Wnt3a*, *Wnt7b*, *Apoe*, and *Gabra5* were hypo-methylated genes in the fetal brain due to *Cav1* ablation. On the other hand, *Fzd2* and *Pou2f2* showed both types of methylations in the fetal brain of *Cav1*-null mice relative to WT mice.

Next, we asked how these metabolism genes differentially methylated in the fetal brain were expressed in the brain of aging mice. RNA-seq was performed to determine gene expression changes of brain of 70-weeks old *Cav1*-null mice compared to age-matched WT mice (accession numbers GEO: GSE215138 and GEO: GSE215139). Differential expression (DE) analysis identified 2,747 genes that were altered significantly (false discovery rate <0.05) in the aging brain of *Cav1*-null compared to WT mice (Table S8). Specific genes (n = 290), henceforth referred to as common DE genes (CDGs), were significantly altered both in fetal as well as aging brain in response to the loss of *Cav1* (Table S9). They included genes that were associated with the deregulated metabolites in the fetal brain, referred to as MDGs, and also genes that were epigenetically altered in the fetal brain, referred to as EDGs (Table S10). We identified groups of CDGs, EDGs, and MDGs that were coordinately activated or suppressed in both the fetal and aging brain due to the loss of *Cav1* (Table S11) suggesting that gene expression pattern in the aging brain of *Cav1*-null mice was linked to the metabolic and epigenetic changes in the fetal brain. To further validate gene expression data, a subset of five genes (*Hspg2*, *Mmp9*, *Igf2*, *Eif3j1*, and *Hbb-bt*) were assayed by quantitative real-time PCR (qRT-PCR) with brain samples from the fetal (GD15) and aged (week 70) from WT and *Cav1*-null mice. The qRT-PCR expression of all the five genes showed similar expression changes as observed from RNA-seq data (Figure S1). The similarity in expression changes was assessed by Pearson correlation coefficients that varied between 0.908 and 0.995.

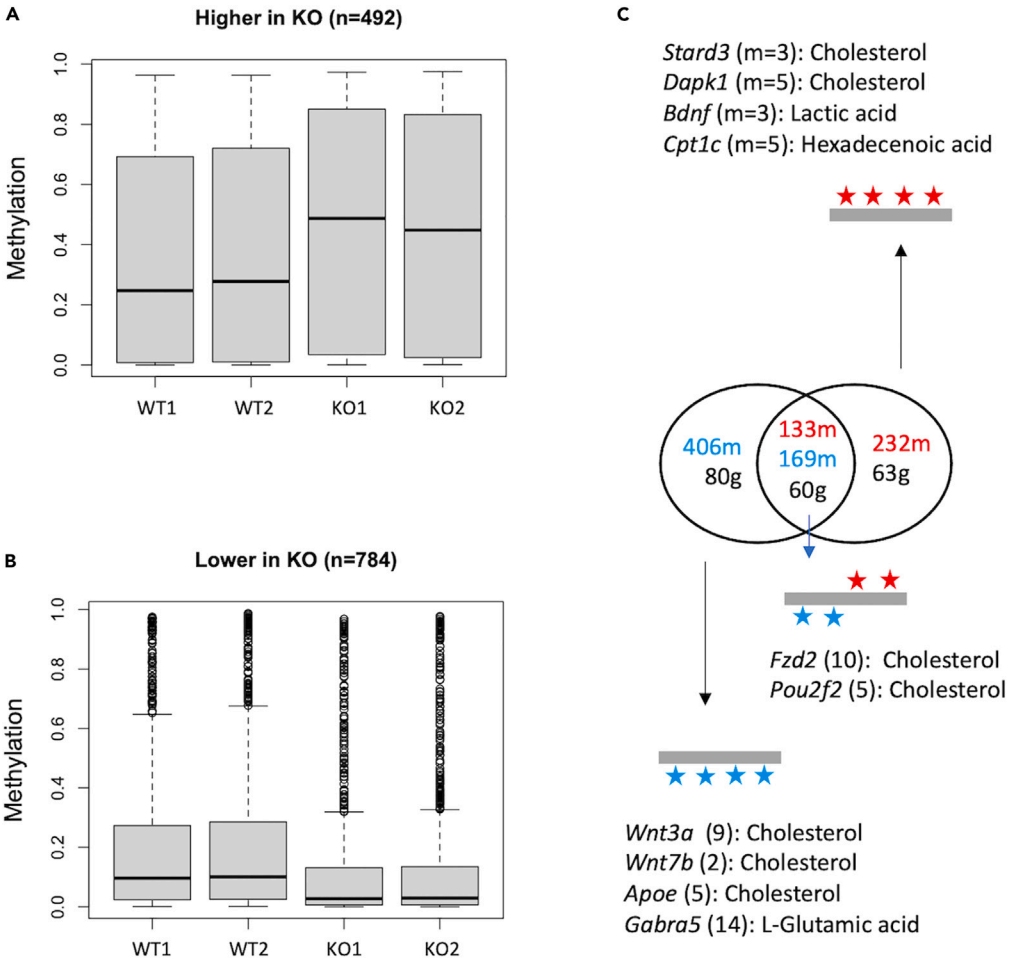

Figure 3. Epigenetic changes of fetal brain and influence on gene expression of aging brain

(A) Higher level of methylation (beta values, shown in y axis) in *Cav1*-null (KO) brain compared to WT brain (female:1, male:2).

(B) Lower level of methylation in *Cav1*-null brain compared to WT brain (female:1, male:2).

(C) In the middle panel, Venn diagram shows the number of methylations (shown as "m") identified in clock genes (shown as "g"). The number of methylations that increased in the fetal brain of *Cav1*-null compared to WT mice is shown in red. The genes are shown as gray bar with red stars (methylations). An opposite pattern was also observed where CpG sites were hypo-methylated in the fetal brain of *Cav1*-null compared to WT mice. The genes are shown as gray bar with blue stars (methylations). In a third group of genes (n = 60), both the types of methylations were observed. They are shown as gray bar (gene) with both red and blue stars (methylations). Specific metabolic genes were identified within these three groups of differentially methylated genes. The gene name, number of methylations (within parenthesis) in the gene, and association with deregulated metabolites are shown.

Identification of cell types and marker genes of WT and Cav1-null fetal brain

We investigated expression patterns of metabolic genes in single cells of the fetal brain from the WT and *Cav1*-null mice. Single-nuclei RNA sequencing (snRNA-seq)[58] was performed to achieve this objective. The snRNA-seq data (accession number GEO: GSE214759) identified a total of 9,544 cells of the WT brain and 10,535 cells of the *Cav1*-null fetal brain. Integrated data analysis of WT and *Cav1*-null snRNA-seq data by *Seurat*[59] identified clusters of neurons, ependymal, radial glia, and microglial cells (Figure 4) based on expression of known marker genes of these cells.[60] The list of marker genes of individual clusters is provided in Table S12. A significant bias (Yates Chi-Square = 174.73, $p < 0.0001$) was observed in the relative number of neuronal and glial cells in the brain of *Cav1*-null compared to WT mice (Figure 5). While the WT brain showed 3,623 neurons and 5,921 glial cells (comprising of radial glia, ependymal, and microglia cells), the *Cav1*-null brain showed 4,974 neurons and 5,561 glial cells. This suggested a change in the relative abundance between neuronal vs. glial cells in the fetal brain due to the loss of *Cav1*. In addition, we observed a significant change (Yates Chi-Square = 149.09, $p < 0.0001$) in the number of ependymal and radial glia cells due to the loss of *Cav1*. A greater number of ependymal cells compared to the radial glial cells were observed in the WT brain, but an opposite pattern was evident in the *Cav1*-null brain. Differential network patterns were observed between neuronal and glial cells in the *Cav1*-null fetal brain compared to the WT brain (Figure S2). In particular, the neuronal and microglial cells showed lower mutual information in gene expression in the *Cav1*-null fetal brain compared to that of the WT brain. Radial glia cells were more abundant in *Cav1*-null compared to the WT brain

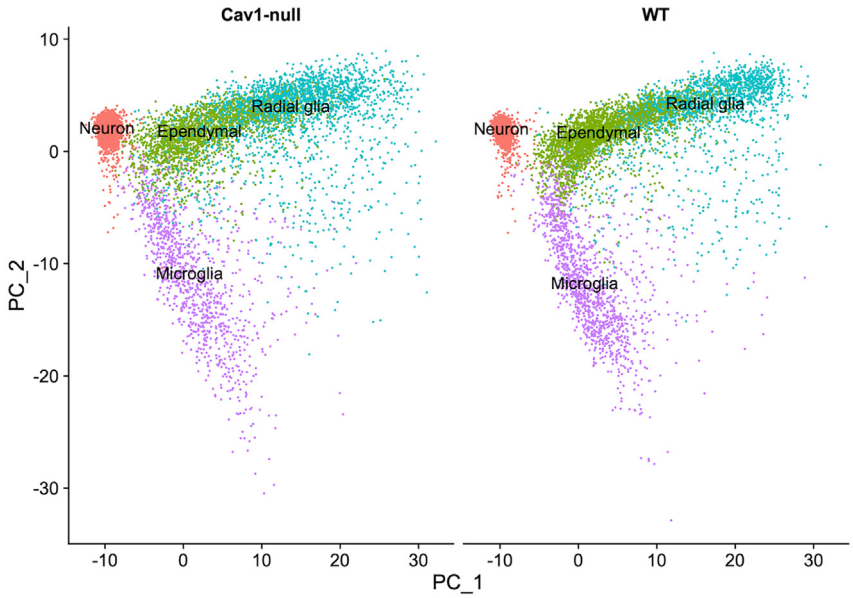

Figure 4. Dimensional plot of single-cell gene expression of *Cav1*-null and WT fetal brain

PC1 and PC2 represent the principal component axes. Each dot represents a cell. Cell types are color coded as shown in the legends.

(Figures 5A and 5B) suggesting a role of *Cav1* in radial glia proliferation. Several metabolic genes associated with lactic acid (LA), L-tyrosine (TY), myo-inositol (MI), glycerophosphate ester (GP), L-glutamic acid (GA), and cholesterol (CH) were identified from snRNA-seq data as cell-specific markers (Table S13). A varying number of metabolic genes were expressed as markers of different cell types between the WT and *Cav1*-null fetal brain (Figure 5C and 5D). The marker genes related to cholesterol were predominantly associated with microglia cells. They included *Bcl2*, *Cdk6*, *Creb5*, *Gli2*, *Gli3*, *Lef1*, *Notch2*, *Plcb1*, *Plpp3*, *Prkca*, *Pbx1*, *Prkd1*, *Runx1t1*, and Tcf7l1 whose expression showed differential hierarchical clustering patterns in the microglia of *Cav1*-null compared to WT mice (Figure S3). The *Runx1t1* gene that controls neuronal differentiation in the developing brain[61] was expressed in the ependymal and radial glia cells at a reduced level in the *Cav1*-null compared to the WT brain (Figure 6). Similarly, *Cntnap2* (contactin-associated protein 2) gene, a major regulator of brain development,[62] was expressed at a reduced level in the radial glia cells of *Cav1*-null compared to the WT brain (Figure 6). Genes related to L-glutamic acid were mostly associated with neurons and radial glia (Table S13). A greater number of L-glutamic acid genes were associated with microglia and ependymal cells of the *Cav1*-null brain compared to the WT brain. These findings collectively suggested that ablation of *Cav1* deregulated specific metabolic genes in specific cell types of the fetal brain.

DISCUSSION

Relevance of metabolic change

The current study showed that lack of *Cav1* perturbed specific metabolites in the fetal brain of mouse. A reduced level of cholesterol was observed in the fetal brain in response to the loss of *Cav1*. Reduced level of cholesterol was also observed in embryonic fibroblasts and peritoneal macrophages of *Cav1*-null mice in an earlier study.[13] The same study[13] further observed that reduction of cholesterol was associated with an increase of acyl-CoA:cholesterol acyl-transferase suggesting a higher level of esterification of cholesterol in response to *Cav1* ablation. However, brain cholesterol is largely independent of circulating cholesterol in the blood due to the blood-brain barrier. Though cholesterol is transported from maternal circulation to the fetal circulation via the placenta,[63] cholesterol is primarily synthesized in the glia cells of the brain.[64] Within neurons, cholesterol homeostasis is controlled by the activation of the oxysterol 24S-hydroxycholesterol (24S-HC) that removes excess cholesterol. In the developing mouse brain, specific nuclear receptors such as liver-X receptors (LXR) play major roles in the regulation of neurogenesis.[65] LXRs can be activated by 24S-HC in the brain[66] that results in the activation of cholesterol transporter *Abca1* to increase efflux of cholesterol from glia.[64] Cholesterol plays critical roles in patterning, myelination, neuronal differentiation, and synaptogenesis during brain development.[67] Deregulation of cholesterol in the fetal brain can also lead to developmental defects of the brain later in life.[34] Besides cholesterol, the metabolomics analysis in the present study showed reduction of palmitic acid and stearic acid but increase of several amino acids in the fetal brain of *Cav1*-null mice. Changes in lipids and amino acids may be associated with the lipid-protein interactions in the brain.[68] Furthermore, the fetal brain of *Cav1*-null mice showed a dramatic increase of urea compared to that of WT mice. Urea is primarily produced in the liver. But urea in the brain is produced by arginine that acts as a substrate for urea cycle.[69] Increased urea level in the brain is associated with age-related brain disorders including Huntington's disease, Parkinson's disease, and Alzheimer's disease.[70–72] It is likely that high level of urea is linked to accelerated aging and early life neurodegeneration known in *Cav1*-null mice.[15]

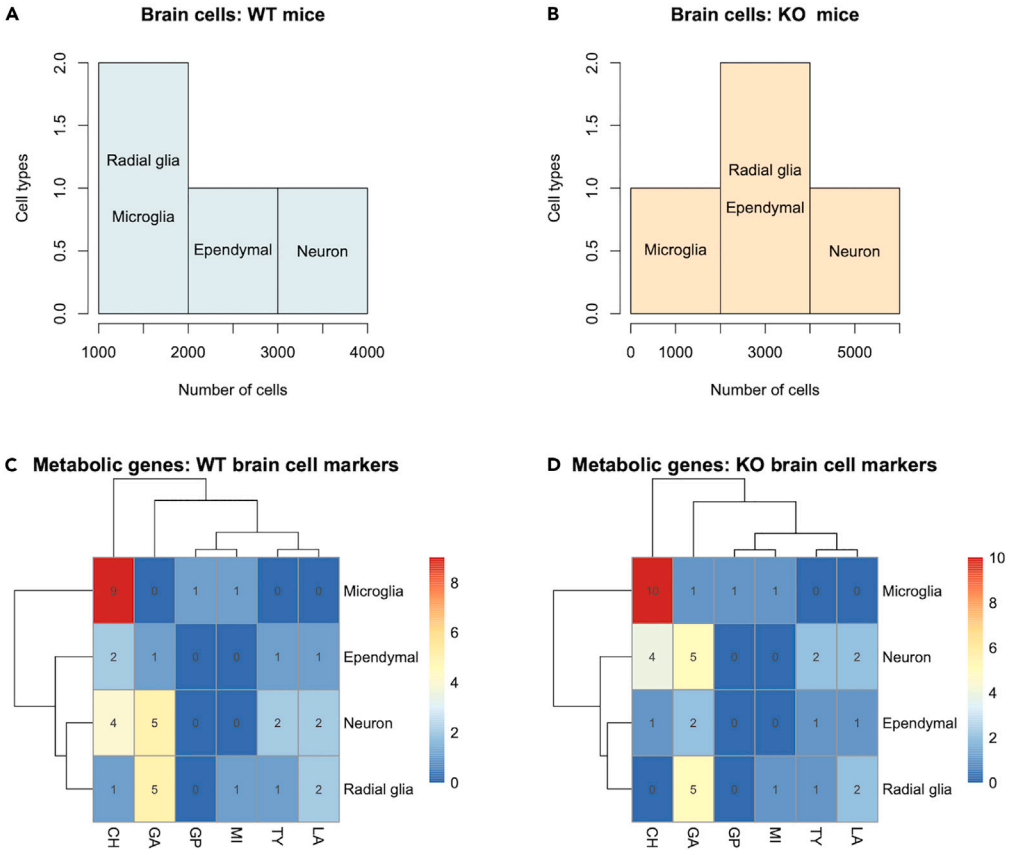

Figure 5. Cell types and metabolic genes as cell specific markers

In the upper panel, the histograms show the differential abundance of glial and neuronal cells in the fetal brain of WT (A) and *Cav1*-null mice (B). In the lower panel, the heatmaps show association of identified marker genes with lactic acid (LA), L-tyrosine (TY), myo-inositol (MI), glycerophosphate ester (GP), L-glutamic acid (GA), and cholesterol (CH) in different cell types of WT (C) and *Cav1*-null fetal brain (D). The scales right to the heatmaps show the color codes for the number of marker genes.

Relevance of metabolism to signaling pathways

Our integrative analysis of metabolomics and gene expression showed that specific metabolite and gene pairs were coordinately upregulated or downregulated in the fetal brain due to the ablation of *Cav1*. These genes and metabolites were commonly associated with specific KEGG pathway modules (a module represents a group of interacting pathways) including beta-oxidation (mmu_M00086), cholesterol biosynthesis (mmu_M00101), and triacylglycerol biosynthesis (mmu_M00089) suggesting role of these pathways in metabolic deregulation of lipids in the *Cav1*-null brain. Fatty acids are generally avoided as energy source for the brain as they demand more oxygen than glucose. Instead, beta-oxidation of glucose is widely used as the major source of energy for brain.[73,74] Stearic acid was the most deregulated lipid in the fetal brain due to loss of *Cav1*. Stearic acid plays a critical role in brain development in mice.[75] Stearic acid along with palmitic acid are significantly altered in the cortex in aging brain.[76] Moreover, brain lipids including cholesterol play influential roles in neuronal aging and aging-related brain disorders.[15,77,78] The increase of urea in the *Cav1*-null brain may be facilitated due to carbamylation[79] which is a post-translational protein modification process via nonenzymatic reaction between isocyanic acid and free amino groups. Carbamylation leads to endothelial dysfunctions that are hallmarks of aging.[79] Therefore, we speculate that high level of urea in the fetal brain of *Cav1*-null mice may cause LDL carbamylation leading to accelerated neuronal aging.[18] In a healthy brain, urea homeostasis is tightly controlled and its deregulation is known to cause pathogenic conditions that eventually lead to dementia.[69–72]

Relevance of receptor-ligand deregulation

Our data also identified specific ligand and receptor genes that were impacted in the fetal brain due to the ablation of *Cav1*. The ligands included apolipoprotein, calmodulin, collagen, fibroblast growth factors, fibronectin, and jagged and G proteins (Table S6). The cognate receptors of these ligands were identified as integrins, fibroblast growth factor receptor, notch, adenylate cyclases. *Apoe* functions as a transporter of cholesterol in the brain[80–82] whereas calcium and calcium-binding proteins (calmodulin) play as regulators of cholesterol metabolism.[83,84] Functional connections of collagen, fibroblast growth factors, and fibronectin with the regulation of cholesterol have been

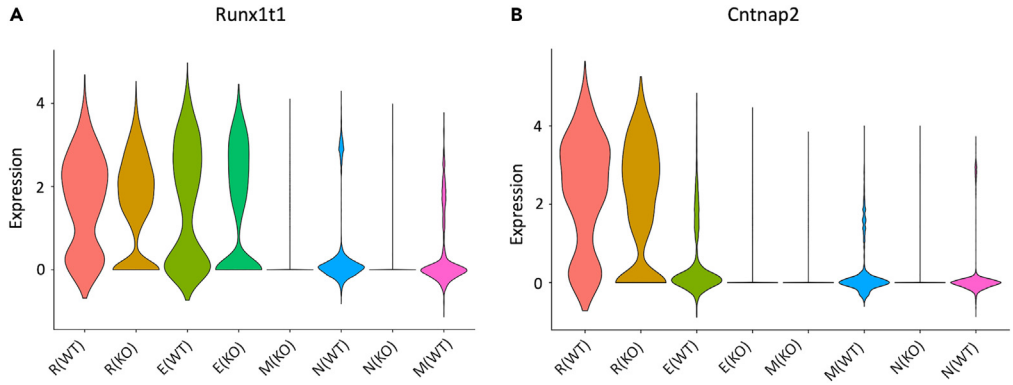

Figure 6. Violin plots showing expression of *Runx1t1* and *Cntnap2* in brain cells of WT (A) and *Cav1*-null mice (B)

X axis shows the cell type and Y axis shows the relative expression values of the integrated data. The cell types in the X axis are abbreviated as R (radial glia), E (ependymal), M (microglia), N (neuron) for both the wild-type (WT) and knockout (KO) samples. The kernel density, wherever applicable, is shown with color.

demonstrated.[85–87] Genes coding for these ligands were downregulated in the *Cav1*-null brain. As abnormal cholesterol level in the brain influences neurodegeneration,[15,88] these findings suggest possible role of cholesterol deregulation in the early life brain aging of *Cav1*-null mice.

Metabolic changes and epigenetic alteration of brain

Within this study, we investigated if genes associated with the deregulated metabolites were epigenetically altered in the brain. We identified several genes including those associated with Wnt signaling that were differentially methylated in the fetal brain of *Cav1*-null mice. Wnt signaling plays important functions during brain development, particularly in neuronal maturation and synaptogenesis.[89] Methylation of Wnt signaling modulates the regulation of prenatal hypoxia of the brain.[90] Wnt signaling genes are deregulated in aging brain as well as in the brain of AD patients.[91] It is likely that epigenetic changes of Wnt signaling genes in *Cav1*-null mice are associated with Alzheimer's disease symptoms observed in these mice at an early age.[15] While some arguments have been made for the use of *Cav1*-null mice as a model for AD,[15] additional studies are needed to support its usefulness as a reliable animal model to study AD pathogenesis in humans.[92] AD pathology depends not only on the formation of amyloid plaques but also on abnormal neurofibrillary tangle.[93] Thus, a better understanding of the role of *Cav1* in both these processes is necessary to determine usefulness of these mice as animal models of AD. There are established mouse models (such as APPSWE, TAU, ARTE10, and humanized APOE) that researchers commonly use in studying human AD. The study by Head et al.[15] suggested that *Cav1* ablation was linked to accelerated neurodegeneration as *Cav1* controls beta-secretase which plays a key role in the production of amyloid beta peptides. We didn't pursue any work to use *Cav1*-null mouse as a model to investigate AD pathogenesis in this study.

The findings of the current study are relevant to the "Latent Early life Associated Regulation" (LEARn) model proposed by Lahiri and Maloney which suggests that changes in the epigenetic state of the brain during early life can be linked to the development of AD pathologies later in life. Links between metabolism and epigenetic changes in fetal brain programming are known.[37,45,45,94] By profiling methylation of mouse epigenetic clock genes,[5] the present study showed that nearly 50% of the CpGs associated with the mouse epigenetic clock were differentially methylated in the fetal brain due to the loss of *Cav1*. We wanted to know how the metabolism genes epigenetically altered in the fetal brain were expressed in the brain at old age. The WT and *Cav1*-null mice were aged to 70 weeks, and brain gene expression was profiled by RNA-seq. The data analysis showed that metabolism genes epigenetically alerted in the fetal brain were differentially regulated in the aging brain. Previous studies have suggested that early life metabolic stresses are epigenetically linked to adult health and diseases.[37] In addition, the role of epigenetics in early life links of aging and longevity has been suggested.[19,95–97] Our recent work suggested that brain aging in mice is programmed by epigenetic changes in the fetal stage.[5] However, further work is needed to confirm if metabolic changes in the fetal brain of *Cav1*-null mice are linked to accelerated aging and neurodegeneration of these mice.

Cav1 and glia-neuron crosstalk

Finally, by performing snRNA-seq, we identified specific cell types that were impacted in the fetal brain due to *Cav1* ablation. The snRNA-seq data showed that the relative abundance of glial and neuronal cells was significantly altered in the fetal brain due to the loss of *Cav1* (Figure 5). In particular, the radial glia cell population was significantly altered in response to *Cav1* ablation. During brain development, radial glial cells play important functions to guide newborn neurons to migrate radially from the ventricular zone to the mantle region. This process is critical for the formation of the cerebral cortex. Recent studies have also shown that these cells regulate gyrification and folding of the cortex[98] as well as pattern formation of the central nervous system.[99] The ependymal cells in the fetal brain play multifaceted function to control the production and flow of cerebrospinal fluid, regulate brain metabolism, and facilitate removal of waste.[100] Deregulated ependyma can impair these process during brain development leading to increased risk for neurodegenerative diseases.[101] *Cav1* is known to influence cell proliferation

and death[11,24,102] by controlling specific apoptosis genes.[103,104] *Cav1* is regarded as a master regulator of cellular senescence.[105] We identified specific genes associated with metabolic pathways (KEGG) of cholesterol, alpha-glycerophosphate ester, myo-inositol, L-glutamic acid, L-tyrosine, and lactic acid that were differentially expressed in specific cells of the fetal brain of *Cav1*-null compared to WT mice (Table S13). The marker genes associated with cholesterol were predominantly expressed in microglia cells, an observation which is consistent to earlier report that high concentrations of cholesterol were required for the survival of microglia.[106] Previous single-cell RNA-seq studies have also shown that specific metabolism genes such as *Trem2*, *Lpl*, and *ApoE* are activated in the microglia that influences metabolic demands during brain development.[81,107,107] In particular, *Trem2* plays a pivotal role in regulating cholesterol metabolism,[81] survival of microglia cells,[108] and mitigating inflammatory responses in the brain.[109]

Limitations of the study

Despite these findings, we consider that our study has limitations. Though methodologies have recently emerged to quantify metabolites in single cells,[110,111] one of the limitations of the present study is the lack of information about metabolite changes in single cells of the brain. However, we were able to determine expression differences of metabolic genes in brain cells in *Cav1*-null relative to the WT brain. The other limitation of the study relates to the mechanisms of how metabolic deregulation can program the fetal brain of *Cav1*-null mice. There may be maternal effects on deregulation of fetal brain metabolism[112,113] that have not been addressed in the current work. However, brain metabolism including that of cholesterol is largely independent from peripheral metabolisms. It is likely that the placenta of *Cav1*-null mice is metabolically deregulated resulting in an abnormal regulation of the brain-placental in these mice. Also, we want to emphasize that although *Cav1*-null mice show certain molecular hallmarks of Alzheimer's disease,[15,114] the present study was not directed to investigate Alzheimer's disease in these mice. Given the biological effect of the large metabolomic effects observed in this study, it is possible that the changes in the metabolites may not be relevant to AD. Future experiments are necessary for biological validation of the omics data of this study relative to AD using established mouse models or *in-vitro* cell culture. Nevertheless, the findings of the present study suggest that abnormality in brain metabolism during fetal life can have profound impacts on the brain during aging.

STAR★METHODS

Detailed methods are provided in the online version of this paper and include the following:

- KEY RESOURCES TABLE
- RESOURCE AVAILABILITY
  - Lead contact
  - Materials availability
  - Data and code availability
- EXPERIMENTAL MODEL AND STUDY PARTICIPANT DETAILS
  - Mice
- METHOD DETAILS
  - Metabolomics analysis of fetal brain
  - Bulk RNA-seq analysis
  - DNA methylation analysis
  - Single-nuclei RNA-seq
  - Data validation
- QUANTIFICATION AND STATISTICAL ANALYSIS

SUPPLEMENTAL INFORMATION

Supplemental information can be found online at https://doi.org/10.1016/j.isci.2023.107710.

ACKNOWLEDGMENTS

This work was supported, in part, by start-up fund from the University of Missouri to SKB. The authors acknowledge the University of Missouri Genomics Technology Core and the Metabolomics Center for the 10X Genomics and metabolomics services, and Ananya Samal and Shankar P Poudel for reading the manuscript.

AUTHOR CONTRIBUTIONS

S.K.B. designed the study, M.I. performed experiments, M.I. and S.K.B. performed data analysis, M.I. and S.K.B. wrote the paper.

DECLARATION OF INTERESTS

The authors declare that they have no competing interests in this research.

Received: March 15, 2023
Revised: May 10, 2023
Accepted: August 23, 2023
Published: August 25, 2023

REFERENCES

1. Greene, N.D.E., and Copp, A.J. (2014). Neural tube defects. Annu. Rev. Neurosci. *37*, 221–242. https://doi.org/10.1146/annurev-neuro-062012-170354.
2. Matcovitch-Natan, O., Winter, D.R., Giladi, A., Vargas Aguilar, S., Spinrad, A., Sarrazin, S., Ben-Yehuda, H., David, E., Zelada González, F., Perrin, P., et al. (2016). Microglia development follows a stepwise program to regulate brain homeostasis. Science *353*, aad8670. https://doi.org/10.1126/science.aad8670.
3. Reemst, K., Noctor, S.C., Lucassen, P.J., and Hol, E.M. (2016). The Indispensable Roles of Microglia and Astrocytes during Brain Development. Front. Hum. Neurosci. *10*, 566. https://doi.org/10.3389/fnhum.2016.00566.
4. Das, S.K. (2009). Cell cycle regulatory control for uterine stromal cell decidualization in implantation. Reproduction *137*, 889–899. https://doi.org/10.1530/REP-08-0539.
5. Islam, M., Strawn, M., and Behura, S.K. (2022). Fetal origin of sex-bias brain aging. Faseb. J. *36*, e22463. https://doi.org/10.1096/fj.202200255RR.
6. Dhakal, P., Strawn, M., Samal, A., and Behura, S.K. (2021). Fetal Brain Elicits Sexually Conflicting Transcriptional Response to the Ablation of Uterine Forkhead Box A2 (Foxa2) in Mice. Int. J. Mol. Sci. *22*, 9693. https://doi.org/10.3390/ijms22189693.
7. Frank, P.G., Woodman, S.E., Park, D.S., and Lisanti, M.P. (2003). Caveolin, caveolae, and endothelial cell function. Arterioscler. Thromb. Vasc. Biol. *23*, 1161–1168. https://doi.org/10.1161/01.ATV.0000070546.16946.3A.
8. Filippini, A., and D'Alessio, A. (2020). Caveolae and Lipid Rafts in Endothelium: Valuable Organelles for Multiple Functions. Biomolecules *10*, 1218. https://doi.org/10.3390/biom10091218.
9. Mohanty, S., Anderson, C.L., and Robinson, J.M. (2010). The expression of caveolin-1 and the distribution of caveolae in the murine placenta and yolk sac: parallels to the human placenta. Placenta *31*, 144–150. https://doi.org/10.1016/j.placenta.2009.11.007.
10. Shikanai, M., Nishimura, Y.V., Sakurai, M., Nabeshima, Y.I., Yuzaki, M., and Kawauchi, T. (2018). Caveolin-1 Promotes Early Neuronal Maturation via Caveolae-Independent Trafficking of N-Cadherin and L1. iScience *7*, 53–67. https://doi.org/10.1016/j.isci.2018.08.014.
11. Silva, W.I., Maldonado, H.M., Velázquez, G., García, J.O., and González, F.A. (2007). Caveolins in glial cell model systems: from detection to significance. J. Neurochem. *103*, 101–112. https://doi.org/10.1111/j.1471-4159.2007.04712.x.
12. Parton, R.G., and del Pozo, M.A. (2013). Caveolae as plasma membrane sensors, protectors and organizers. Nat. Rev. Mol. Cell Biol. *14*, 98–112. https://doi.org/10.1038/nrm3512.
13. Razani, B., Engelman, J.A., Wang, X.B., Schubert, W., Zhang, X.L., Marks, C.B., Macaluso, F., Russell, R.G., Li, M., Pestell, R.G., et al. (2001). Caveolin-1 Null Mice Are Viable but Show Evidence of Hyperproliferative and Vascular Abnormalities. J. Biol. Chem. *276*, 38121–38138. https://doi.org/10.1074/jbc.M105408200.
14. Park, D.S., Cohen, A.W., Frank, P.G., Razani, B., Lee, H., Williams, T.M., Chandra, M., Shirani, J., De Souza, A.P., Tang, B., et al. (2003). Caveolin-1 null (-/-) mice show dramatic reductions in life span. Biochemistry *42*, 15124–15131. https://doi.org/10.1021/bi0356348.
15. Head, B.P., Peart, J.N., Panneerselvam, M., Yokoyama, T., Pearn, M.L., Niesman, I.R., Bonds, J.A., Schilling, J.M., Miyanohara, A., Headrick, J., et al. (2010). Loss of caveolin-1 accelerates neurodegeneration and aging. PLoS One *5*, e15697. https://doi.org/10.1371/journal.pone.0015697.
16. Schlegel, A., Arvan, P., and Lisanti, M.P. (2001). Caveolin-1 binding to endoplasmic reticulum membranes and entry into the regulated secretory pathway are regulated by serine phosphorylation. Protein sorting at the level of the endoplasmic reticulum. J. Biol. Chem. *276*, 4398–4408. https://doi.org/10.1074/jbc.M005448200.
17. Lemche, E. (2018). Early Life Stress and Epigenetics in Late-onset Alzheimer's Dementia: A Systematic Review. Curr. Genom. *19*, 522–602. https://doi.org/10.2174/1389202919666171229145156.
18. Lesuis, S.L., van Hoek, B.A.C.E., Lucassen, P.J., and Krugers, H.J. (2017). Early postnatal handling reduces hippocampal amyloid plaque formation and enhances cognitive performance in APPswe/PS1dE9 mice at middle age. Neurobiol. Learn. Mem. *144*, 27–35. https://doi.org/10.1016/j.nlm.2017.05.016.
19. Hadad, N., Masser, D.R., Blanco-Berdugo, L., Stanford, D.R., and Freeman, W.M. (2019). Early-life DNA methylation profiles are indicative of age-related transcriptome changes. Epigenet. Chromatin *12*, 58. https://doi.org/10.1186/s13072-019-0306-5.
20. Lesuis, S.L., Hoeijmakers, L., Korosi, A., de Rooij, S.R., Swaab, D.F., Kessels, H.W., Lucassen, P.J., and Krugers, H.J. (2018). Vulnerability and resilience to Alzheimer's disease: early life conditions modulate neuropathology and determine cognitive reserve. Alzheimer's Res. Ther. *10*, 95. https://doi.org/10.1186/s13195-018-0422-7.
21. Lahiri, D.K., and Maloney, B. (2010). The "LEARn" (Latent Early-life Associated Regulation) model integrates environmental risk factors and the developmental basis of Alzheimer's disease, and proposes remedial steps. Exp. Gerontol. *45*, 291–296. https://doi.org/10.1016/j.exger.2010.01.001.
22. Breuer, M., Berger, H., and Borchers, A. (2020). Caveolin 1 is required for axonal outgrowth of motor neurons and affects Xenopus neuromuscular development. Sci. Rep. *10*, 16446. https://doi.org/10.1038/s41598-020-73429-x.
23. Head, B.P., and Insel, P.A. (2007). Do caveolins regulate cells by actions outside of caveolae? Trends Cell Biol. *17*, 51–57. https://doi.org/10.1016/j.tcb.2006.11.008.
24. Sandhu, J.K., Ribecco-Lutkiewicz, M., and Abulrob, A. (2021). Molecular and Functional Characterization of Caveolae in Mixed Cultures of Human NT-2 Neurons and Astrocytes. Neuroglia *2*, 68–88. https://doi.org/10.3390/neuroglia2010008.
25. Frank, P.G., Cheung, M.W.-C., Pavlides, S., Llaverias, G., Park, D.S., and Lisanti, M.P. (2006). Caveolin-1 and regulation of cellular cholesterol homeostasis. Am. J. Physiol. Heart Circ. Physiol. *291*, H677–H686. https://doi.org/10.1152/ajpheart.01092.2005.
26. Raudenska, M., Gumulec, J., Balvan, J., and Masarik, M. (2020). Caveolin-1 in oncogenic metabolic symbiosis. Int. J. Cancer *147*, 1793–1807. https://doi.org/10.1002/ijc.32987.
27. Luo, S., Yang, M., Zhao, H., Han, Y., Jiang, N., Yang, J., Chen, W., Li, C., Liu, Y., Zhao, C., and Sun, L. (2021). Caveolin-1 Regulates Cellular Metabolism: A Potential Therapeutic Target in Kidney Disease. Front. Pharmacol. *12*, 768100.
28. Han, M., Piorońska, W., Yang, P., Zhong, C., Chen, C., Wang, S., Lu, Q., Ning, K., Dooley, S., and Meyer, C. (2020). Hepatocyte caveolin-1 modulates metabolic gene profiles and functions in non-alcoholic fatty liver disease. Gut Microb. *12*, 1–18. https://doi.org/10.1038/s41419-020-2295-5.
29. Feng, X., Huang, H., Yang, Y., Fröhlich, O., Klein, J.D., Sands, J.M., and Chen, G. (2009). Caveolin-1 directly interacts with UT-A1 urea transporter: the role of caveolae/lipid rafts in UT-A1 regulation at the cell membrane. Am. J. Physiol. Ren. Physiol. *296*, F1514–F1520. https://doi.org/10.1152/ajprenal.00068.
30. Zhang, X., Li, L., Zhang, X., Xie, W., Li, L., Yang, D., Heng, X., Du, Y., Doody, R.S., and Le, W. (2013). Prenatal hypoxia may aggravate the cognitive impairment and Alzheimer's disease neuropathology in APPSwe/PS1A246E transgenic mice. Neurobiol. Aging *34*, 663–678. https://doi.org/10.1016/j.neurobiolaging.2012.06.012.
31. Faa, G., Marcialis, M.A., Ravarino, A., Piras, M., Pintus, M.C., and Fanos, V. (2014). Fetal programming of the human brain: is there a link with insurgence of neurodegenerative disorders in adulthood? Curr. Med. Chem. *21*, 3854–3876. https://doi.org/10.2174/09298673216661406011636 58.
32. Deems, N.P., and Leuner, B. (2020). Pregnancy, postpartum and parity: Resilience and vulnerability in brain health and disease. Front. Neuroendocrinol. *57*, 100820. https://doi.org/10.1016/j.yfrne.2020.100820.
33. Shen, G., Hu, S., Zhao, Z., Zhang, L., and Ma, Q. (2020). Antenatal Hypoxia Accelerates the Onset of Alzheimer's Disease Pathology in 5xFAD Mouse Model. Front. Aging

Neurosci. *12*, 251. https://doi.org/10.3389/fnagi.2020.00251.
34. Martín, M.G., Pfrieger, F., and Dotti, C.G. (2014). Cholesterol in brain disease: sometimes determinant and frequently implicated. EMBO Rep. *15*, 1036–1052. https://doi.org/10.15252/embr.201439225.
35. Souza, L.L., de Moura, E.G., and Lisboa, P.C. (2020). Does early weaning shape future endocrine and metabolic disorders? Lessons from animal models. J. Dev. Orig. Health Dis. *11*, 441–451. https://doi.org/10.1017/S2040174420000410.
36. Carson, C., and Lawson, H.A. (2018). Epigenetics of metabolic syndrome. Physiol. Genom. *50*, 947–955. https://doi.org/10.1152/physiolgenomics.00072.2018.
37. Bouchard, L. (2013). Epigenetics and Fetal Metabolic Programming: A Call for Integrated Research on Larger Cohorts. Diabetes *62*, 1026–1028. https://doi.org/10.2337/db12-1763.
38. Tzika, E., Dreker, T., and Imhof, A. (2018). Epigenetics and Metabolism in Health and Disease. Front. Genet. *9*, 361. https://doi.org/10.3389/fgene.2018.00361.
39. Mochizuki, K., Hariya, N., Honma, K., and Goda, T. (2017). Relationship between epigenetic regulation, dietary habits, and the developmental origins of health and disease theory. Congenital. Anom. *57*, 184–190. https://doi.org/10.1111/cga.12213.
40. D'Urso, A., and Brickner, J.H. (2014). Mechanisms of epigenetic memory. Trends Genet. *30*, 230–236. https://doi.org/10.1016/j.tig.2014.04.004.
41. Thiagalingam, S. (2020). Epigenetic memory in development and disease: unraveling the mechanism. Biochim. Biophys. Acta Rev. Canc *1873*, 188349. https://doi.org/10.1016/j.bbcan.2020.188349.
42. Yu, V.W.C., Yusuf, R.Z., Oki, T., Wu, J., Saez, B., Wang, X., Cook, C., Baryawno, N., Ziller, M.J., Lee, E., et al. (2017). Epigenetic Memory Underlies Cell-Autonomous Heterogeneous Behavior of Hematopoietic Stem Cells. Cell *168*, 944–945. https://doi.org/10.1016/j.cell.2017.02.010.
43. Goyal, D., Limesand, S.W., and Goyal, R. (2019). Epigenetic responses and the developmental origins of health and disease. J. Endocrinol. *242*, T105–T119. https://doi.org/10.1530/JOE-19-0009.
44. Hoffman, D.J., Reynolds, R.M., and Hardy, D.B. (2017). Developmental origins of health and disease: current knowledge and potential mechanisms. Nutr. Rev. *75*, 951–970. https://doi.org/10.1093/nutrit/nux053.
45. Wadhwa, P.D., Buss, C., Entringer, S., and Swanson, J.M. (2009). Developmental Origins of Health and Disease: Brief History of the Approach and Current Focus on Epigenetic Mechanisms. Semin. Reprod. Med. *27*, 358–368. https://doi.org/10.1055/s-0029-1237424.
46. Sotgia, F., Del Galdo, F., Casimiro, M.C., Bonuccelli, G., Mercier, I., Whitaker-Menezes, D., Daumer, K.M., Zhou, J., Wang, C., Katiyar, S., et al. (2009). Caveolin-1−/− Null Mammary Stromal Fibroblasts Share Characteristics with Human Breast Cancer-Associated Fibroblasts. Am. J. Pathol. *174*, 746–761. https://doi.org/10.2353/ajpath.2009.080658.
47. Park, D.S., Lee, H., Frank, P.G., Razani, B., Nguyen, A.V., Parlow, A.F., Russell, R.G., Hulit, J., Pestell, R.G., and Lisanti, M.P. (2002). Caveolin-1-deficient Mice Show Accelerated Mammary Gland Development During Pregnancy, Premature Lactation, and Hyperactivation of the Jak-2/STAT5a Signaling Cascade. Mol. Biol. Cell *13*, 3416–3430. https://doi.org/10.1091/mbc.02-05-0071.
48. Shiroto, T., Romero, N., Sugiyama, T., Sartoretto, J.L., Kalwa, H., Yan, Z., Shimokawa, H., and Michel, T. (2014). Caveolin-1 is a critical determinant of autophagy, metabolic switching, and oxidative stress in vascular endothelium. PLoS One *9*, e87871. https://doi.org/10.1371/journal.pone.0087871.
49. Buchholz, A.C., Rafii, M., and Pencharz, P.B. (2001). Is resting metabolic rate different between men and women? Br. J. Nutr. *86*, 641–646. https://doi.org/10.1079/bjn2001471.
50. Cheng, Y., and Church, G.M. (2000). Biclustering of expression data. Proc. Int. Conf. Intell. Syst. Mol. Biol. *8*, 93–103.
51. Zhuang, X., Yang, Z., and Cordes, D. (2020). A technical review of canonical correlation analysis for neuroscience applications. Hum. Brain Mapp. *41*, 3807–3833. https://doi.org/10.1002/hbm.25090.
52. Wilms, I., and Croux, C. (2015). Sparse canonical correlation analysis from a predictive point of view. Biom. J. *57*, 834–851. https://doi.org/10.1002/bimj.201400226.
53. Meyer, P.E., Lafitte, F., and Bontempi, G. (2008). minet: A R/Bioconductor package for inferring large transcriptional networks using mutual information. BMC Bioinf. *9*, 461. https://doi.org/10.1186/1471-2105-9-461.
54. Koschützki, D., and Schreiber, F. (2008). Centrality Analysis Methods for Biological Networks and Their Application to Gene Regulatory Networks. Gene Regul. Syst. Biol. *2*, 193–201.
55. Ramilowski, J.A., Goldberg, T., Harshbarger, J., Kloppmann, E., Lizio, M., Satagopam, V.P., Itoh, M., Kawaji, H., Carninci, P., Rost, B., and Forrest, A.R.R. (2015). A draft network of ligand-receptor-mediated multicellular signalling in human. Nat. Commun. *6*, 7866. https://doi.org/10.1038/ncomms8866.
56. Behura, S.K., Kelleher, A.M., and Spencer, T.E. (2019). Evidence for functional interactions between the placenta and brain in pregnant mice. Faseb. J. *33*, 4261–4272. https://doi.org/10.1096/fj.201802037R.
57. Stubbs, T.M., Bonder, M.J., Stark, A.-K., Krueger, F., Reik, W., BI Ageing Clock Team, von Meyenn, F., and Stegle, O. (2017). Multi-tissue DNA methylation age predictor in mouse. Genome Biol. *18*, 68. https://doi.org/10.1186/s13059-017-1203-5.
58. Grindberg, R.V., Yee-Greenbaum, J.L., McConnell, M.J., Novotny, M., O'Shaughnessy, A.L., Lambert, G.M., Araúzo-Bravo, M.J., Lee, J., Fishman, M., Robbins, G.E., et al. (2013). RNA-sequencing from single nuclei. Proc. Natl. Acad. Sci. USA *110*, 19802–19807. https://doi.org/10.1073/pnas.1319700110.
59. Butler, A., Hoffman, P., Smibert, P., Papalexi, E., and Satija, R. (2018). Integrating single-cell transcriptomic data across different conditions, technologies, and species. Nat. Biotechnol. *36*, 411–420. https://doi.org/10.1038/nbt.4096.
60. Franzén, O., Gan, L.-M., and Björkegren, J.L.M. (2019). PanglaoDB: a web server for exploration of mouse and human single-cell RNA sequencing data. Database *2019*, baz046. https://doi.org/10.1093/database/baz046.
61. Zou, L., Li, H., Han, X., Qin, J., and Song, G. (2020). Runx1t1 promotes the neuronal differentiation in rat hippocampus. Stem Cell Res. Ther. *11*, 160. https://doi.org/10.1186/s13287-020-01667-x.
62. Scott, R., Sánchez-Aguilera, A., van Elst, K., Lim, L., Dehorter, N., Bae, S.E., Bartolini, G., Peles, E., Kas, M.J.H., Bruining, H., and Marín, O. (2019). Loss of Cntnap2 Causes Axonal Excitability Deficits, Developmental Delay in Cortical Myelination, and Abnormal Stereotyped Motor Behavior. Cerebr. Cortex *29*, 586–597. https://doi.org/10.1093/cercor/bhx341.
63. Yoshida, S., and Wada, Y. (2005). Transfer of maternal cholesterol to embryo and fetus in pregnant mice. J. Lipid Res. *46*, 2168–2174. https://doi.org/10.1194/jlr.M500096-JLR200.
64. Björkhem, I., and Meaney, S. (2004). Brain cholesterol: long secret life behind a barrier. Arterioscler. Thromb. Vasc. Biol. *24*, 806–815. https://doi.org/10.1161/01.ATV.0000120374.59826.1b.
65. Janowski, B.A., Willy, P.J., Devi, T.R., Falck, J.R., and Mangelsdorf, D.J. (1996). An oxysterol signalling pathway mediated by the nuclear receptor LXR alpha. Nature *383*, 728–731. https://doi.org/10.1038/383728a0.
66. Zhang, J., Zhang, F., Wu, J., Li, J., Yang, Z., and Yue, J. (2020). Glutamate affects cholesterol homeostasis within the brain via the up-regulation of CYP46A1 and ApoE. Toxicology *432*, 152381. https://doi.org/10.1016/j.tox.2020.152381.
67. Lu, F., Ferriero, D.M., and Jiang, X. (2022). Cholesterol in Brain Development and Perinatal Brain Injury: More than a Building Block. Curr. Neuropharmacol. *20*, 1400–1412. https://doi.org/10.2174/1570159X19666211111122311.
68. Chattopadhyay, A., and Paila, Y.D. (2007). Lipid-protein interactions, regulation and dysfunction of brain cholesterol. Biochem. Biophys. Res. Commun. *354*, 627–633. https://doi.org/10.1016/j.bbrc.2007.01.032.
69. Gropman, A.L., Summar, M., and Leonard, J.V. (2007). Neurological implications of urea cycle disorders. J. Inherit. Metab. Dis. *30*, 865–879. https://doi.org/10.1007/s10545-007-0709-5.
70. Hansmannel, F., Sillaire, A., Kamboh, M.I., Lendon, C., Pasquier, F., Hannequin, D., Laumet, G., Mounier, A., Ayral, A.-M., DeKosky, S.T., et al. (2010). Is the urea cycle involved in Alzheimer's disease? J. Alzheimers Dis. *21*, 1013–1021. https://doi.org/10.3233/JAD-2010-100630.
71. Scholefield, M., Church, S.J., Xu, J., Patassini, S., Roncaroli, F., Hooper, N.M., Unwin, R.D., and Cooper, G.J.S. (2021). Severe and Regionally Widespread Increases in Tissue Urea in the Human Brain Represent a Novel Finding of Pathogenic Potential in Parkinson's Disease Dementia. Front. Mol. Neurosci. *14*, 711396. https://doi.org/10.3389/fnmol.2021.711396.
72. Handley, R.R., Reid, S.J., Brauning, R., Maclean, P., Mears, E.R., Fourie, I., Patassini, S., Cooper, G.J.S., Rudiger, S.R., McLaughlan, C.J., et al. (2017). Brain urea increase is an early Huntington's disease pathogenic event observed in a prodromal transgenic sheep model and HD cases.

Proc. Natl. Acad. Sci. USA *114*, E11293–E11302. https://doi.org/10.1073/pnas.1711243115.

73. Schönfeld, P., and Reiser, G. (2013). Why does brain metabolism not favor burning of fatty acids to provide energy? - Reflections on disadvantages of the use of free fatty acids as fuel for brain. J. Cerebr. Blood Flow Metabol. *33*, 1493–1499. https://doi.org/10.1038/jcbfm.2013.128.
74. Steiner, P. (2019). Brain Fuel Utilization in the Developing Brain. Ann. Nutr. Metab. *75* (*Suppl 1*), 8–18. https://doi.org/10.1159/000508054.
75. Gozlan-Devillierre, N., Baumann, N., and Bourre, J.M. (1978). Incorporation of stearic acid into brain lipids in the developing brain: blood-brain relationships during development. Dev. Neurosci. *1*, 153–158. https://doi.org/10.1159/000112567.
76. Patil, S., and Chan, C. (2005). Palmitic and stearic fatty acids induce Alzheimer-like hyperphosphorylation of tau in primary rat cortical neurons. Neurosci. Lett. *384*, 288–293. https://doi.org/10.1016/j.neulet.2005.05.003.
77. Martin, M., Dotti, C.G., and Ledesma, M.D. (2010). Brain cholesterol in normal and pathological aging. Biochim. Biophys. Acta *1801*, 934–944. https://doi.org/10.1016/j.bbalip.2010.03.011.
78. Nunes, V.S., da Silva Ferreira, G., and Quintão, E.C.R. (2022). Cholesterol metabolism in aging simultaneously altered in liver and nervous system. Aging (Albany NY) *14*, 1549–1561. https://doi.org/10.18632/aging.203880.
79. Basnakian, A.G., Shah, S.V., Ok, E., Altunel, E., and Apostolov, E.O. (2010). Carbamylated LDL. Adv. Clin. Chem. *51*, 25–52. https://doi.org/10.1016/s0065-2423(10)51002-3.
80. Martins, I.J., Hone, E., Foster, J.K., Sünram-Lea, S.I., Gnjec, A., Fuller, S.J., Nolan, D., Gandy, S.E., and Martins, R.N. (2006). Apolipoprotein E, cholesterol metabolism, diabetes, and the convergence of risk factors for Alzheimer's disease and cardiovascular disease. Mol. Psychiatr. *11*, 721–736. https://doi.org/10.1038/sj.mp.4001854.
81. Nugent, A.A., Lin, K., van Lengerich, B., Lianoglou, S., Przybyla, L., Davis, S.S., Llapashtica, C., Wang, J., Kim, D.J., Xia, D., et al. (2020). TREM2 Regulates Microglial Cholesterol Metabolism upon Chronic Phagocytic Challenge. Neuron *105*, 837–854.e9. https://doi.org/10.1016/j.neuron.2019.12.007.
82. Vance, J.E. (2012). Dysregulation of cholesterol balance in the brain: contribution to neurodegenerative diseases. Dis. Model. Mech. *5*, 746–755. https://doi.org/10.1242/dmm.010124.
83. Nishizawa, Y., Okui, Y., Inaba, M., Okuno, S., Yukioka, K., Miki, T., Watanabe, Y., and Morii, H. (1988). Calcium/calmodulin-mediated action of calcitonin on lipid metabolism in rats. J. Clin. Invest. *82*, 1165–1172. https://doi.org/10.1172/JCI113713.
84. Ortega, A., and Mas-Oliva, J. (1986). Direct regulatory effect of cholesterol on the calmodulin stimulated calcium pump of cardiac sarcolemma. Biochem. Biophys. Res. Commun. *139*, 868–874. https://doi.org/10.1016/s0006-291x(86)80258-3.
85. Cicchi, R., Matthäus, C., Meyer, T., Lattermann, A., Dietzek, B., Brehm, B.R., Popp, J., and Pavone, F.S. (2014). Characterization of collagen and cholesterol deposition in atherosclerotic arterial tissue using non-linear microscopy. J. Biophot. *7*, 135–143. https://doi.org/10.1002/jbio.201300055.
86. Chijiiwa, K., Koga, A., Yamasaki, T., Shimada, K., Noshiro, H., and Nakayama, F. (1991). Fibronectin: a possible factor promoting cholesterol monohydrate crystallization in bile. Biochim. Biophys. Acta *1086*, 44–48. https://doi.org/10.1016/0005-2760(91)90152-8.
87. Shang, W., Yu, X., Wang, H., Chen, T., Fang, Y., Yang, X., Zhou, P., Nie, F., Zhou, Q., and Zhou, J. (2015). Fibroblast growth factor 21 enhances cholesterol efflux in THP-1 macrophage-derived foam cells. Mol. Med. Rep. *11*, 503–508. https://doi.org/10.3892/mmr.2014.2731.
88. Petrov, A.M., Kasimov, M.R., and Zefirov, A.L. (2016). Brain Cholesterol Metabolism and Its Defects: Linkage to Neurodegenerative Diseases and Synaptic Dysfunction. Acta Naturae *8*, 58–73.
89. Noelanders, R., and Vleminckx, K. (2017). How Wnt Signaling Builds the Brain: Bridging Development and Disease. Neuroscientist *23*, 314–329. https://doi.org/10.1177/1073858416667270.
90. Zhang, Y., Zhang, M., Li, L., Wei, B., He, A., Lu, L., Li, X., Zhang, L., Xu, Z., and Sun, M. (2018). Methylation-reprogrammed Wnt/β-catenin signalling mediated prenatal hypoxia-induced brain injury in foetal and offspring rats. J. Cell Mol. Med. *22*, 3866–3874. https://doi.org/10.1111/jcmm.13660.
91. Palomer, E., Buechler, J., and Salinas, P.C. (2019). Wnt Signaling Deregulation in the Aging and Alzheimer's Brain. Front. Cell. Neurosci. *13*, 227. https://doi.org/10.3389/fncel.2019.00227.
92. Hall, A.M., and Roberson, E.D. (2012). Mouse Models of Alzheimer's Disease. Brain Res. Bull. *88*, 3–12. https://doi.org/10.1016/j.brainresbull.2011.11.017.
93. Drummond, E., and Wisniewski, T. (2017). Alzheimer's Disease: Experimental Models and Reality. Acta Neuropathol. *133*, 155–175. https://doi.org/10.1007/s00401-016-1662-x.
94. Chmurzynska, A. (2010). Fetal programming: link between early nutrition, DNA methylation, and complex diseases. Nutr. Rev. *68*, 87–98. https://doi.org/10.1111/j.1753-4887.2009.00265.x.
95. Babenko, O., Kovalchuk, I., and Metz, G.A.S. (2015). Stress-induced perinatal and transgenerational epigenetic programming of brain development and mental health. Neurosci. Biobehav. Rev. *48*, 70–91. https://doi.org/10.1016/j.neubiorev.2014.11.013.
96. Numata, S., Ye, T., Hyde, T.M., Guitart-Navarro, X., Tao, R., Wininger, M., Colantuoni, C., Weinberger, D.R., Kleinman, J.E., and Lipska, B.K. (2012). DNA Methylation Signatures in Development and Aging of the Human Prefrontal Cortex. Am. J. Hum. Genet. *90*, 260–272. https://doi.org/10.1016/j.ajhg.2011.12.020.
97. Ben-Avraham, D. (2015). Epigenetics of aging. Adv. Exp. Med. Biol. *847*, 179–191. https://doi.org/10.1007/978-1-4939-2404-2_9.
98. Borrell, V., and Götz, M. (2014). Role of radial glial cells in cerebral cortex folding. Curr. Opin. Neurobiol. *27*, 39–46. https://doi.org/10.1016/j.conb.2014.02.007.
99. Campbell, K., and Götz, M. (2002). Radial glia: multi-purpose cells for vertebrate brain development. Trends Neurosci. *25*, 235–238. https://doi.org/10.1016/s0166-2236(02)02156-2.
100. Deng, S., Gan, L., Liu, C., Xu, T., Zhou, S., Guo, Y., Zhang, Z., Yang, G.-Y., Tian, H., and Tang, Y. (2023). Roles of Ependymal Cells in the Physiology and Pathology of the Central Nervous System. Aging Dis. *14*, 468–483. https://doi.org/10.14336/AD.2022.0826-1.
101. Nelles, D.G., and Hazrati, L.-N. (2022). Ependymal cells and neurodegenerative disease: outcomes of compromised ependymal barrier function. Brain Commun. *4*, fcac288. https://doi.org/10.1093/braincomms/fcac288.
102. Wang, F., Cao, Y., Ma, L., Pei, H., Rausch, W.D., and Li, H. (2018). Dysfunction of Cerebrovascular Endothelial Cells: Prelude to Vascular Dementia. Front. Aging Neurosci. *10*, 376.
103. Torres, V.A., Tapia, J.C., Rodríguez, D.A., Párraga, M., Lisboa, P., Montoya, M., Leyton, L., and Quest, A.F.G. (2006). Caveolin-1 controls cell proliferation and cell death by suppressing expression of the inhibitor of apoptosis protein survivin. J. Cell Sci. *119*, 1812–1823. https://doi.org/10.1242/jcs.02894.
104. Jasmin, J.-F., Malhotra, S., Singh Dhallu, M., Mercier, I., Rosenbaum, D.M., and Lisanti, M.P. (2007). Caveolin-1 deficiency increases cerebral ischemic injury. Circ. Res. *100*, 721–729. https://doi.org/10.1161/01.RES.0000260180.42709.29.
105. Volonte, D., and Galbiati, F. (2020). Caveolin-1, a master regulator of cellular senescence. Cancer Metastasis Rev. *39*, 397–414. https://doi.org/10.1007/s10555-020-09875-w.
106. Bohlen, C.J., Bennett, F.C., Tucker, A.F., Collins, H.Y., Mulinyawe, S.B., and Barres, B.A. (2017). Diverse Requirements for Microglial Survival, Specification, and Function Revealed by Defined-Medium Cultures. Neuron *94*, 759–773.e8. https://doi.org/10.1016/j.neuron.2017.04.043.
107. Loving, B.A., and Bruce, K.D. (2020). Lipid and Lipoprotein Metabolism in Microglia. Front. Physiol. *11*, 393.
108. Zheng, H., Jia, L., Liu, C.-C., Rong, Z., Zhong, L., Yang, L., Chen, X.-F., Fryer, J.D., Wang, X., Zhang, Y.W., et al. (2017). TREM2 Promotes Microglial Survival by Activating Wnt/β-Catenin Pathway. J. Neurosci. *37*, 1772–1784. https://doi.org/10.1523/JNEUROSCI.2459-16.2017.
109. Xu, X., Du, L., Jiang, J., Yang, M., Wang, Z., Wang, Y., Tang, T., Fu, X., and Hao, J. (2021). Microglial TREM2 Mitigates Inflammatory Responses and Neuronal Apoptosis in Angiotensin II-Induced Hypertension in Middle-Aged Mice. Front. Aging Neurosci. *13*, 716917. https://doi.org/10.3389/fnagi.2021.716917.
110. Duncan, K.D., Fyrestam, J., and Lanekoff, I. (2019). Advances in mass spectrometry based single-cell metabolomics. Analyst *144*, 782–793. https://doi.org/10.1039/c8an01581c.
111. Lanekoff, I., Sharma, V.V., and Marques, C. (2022). Single-cell metabolomics: where are we and where are we going? Curr. Opin. Biotechnol. *75*, 102693. https://doi.org/10.1016/j.copbio.2022.102693.
112. Cheatham, C.L. (2019). Nutritional Factors in Fetal and Infant Brain Development. Ann. Nutr. Metab. *75*, 20–32. https://doi.org/10.1159/000508052.

113. Goeden, N., Velasquez, J., Arnold, K.A., Chan, Y., Lund, B.T., Anderson, G.M., and Bonnin, A. (2016). Maternal Inflammation Disrupts Fetal Neurodevelopment via Increased Placental Output of Serotonin to the Fetal Brain. J. Neurosci. *36*, 6041–6049. https://doi.org/10.1523/JNEUROSCI.2534-15.2016.

114. van Helmond, Z.K., Miners, J.S., Bednall, E., Chalmers, K.A., Zhang, Y., Wilcock, G.K., Love, S., and Kehoe, P.G. (2007). Caveolin-1 and -2 and their relationship to cerebral amyloid angiopathy in Alzheimer's disease. Neuropathol. Appl. Neurobiol. *33*, 317–327. https://doi.org/10.1111/j.1365-2990.2006.00815.x.

115. Broeckling, C.D., Reddy, I.R., Duran, A.L., Zhao, X., and Sumner, L.W. (2006). MET-IDEA: data extraction tool for mass spectrometry-based metabolomics. Anal. Chem. *78*, 4334–4341. https://doi.org/10.1021/ac0521596.

116. Behura, S.K., Kelleher, A.M., and Spencer, T.E. (2020). Regulation of uterine genes during the peri-implantation period, and its relationship to the maternal brain in gestating mice. Mol. Reprod. Dev. *87*, 482–492. https://doi.org/10.1002/mrd.23338.

117. Strawn, M., Moraes, J.G.N., Safranski, T.J., and Behura, S.K. (2021). Sexually Dimorphic Transcriptomic Changes of Developing Fetal Brain Reveal Signaling Pathways and Marker Genes of Brain Cells in Domestic Pigs. Cells *10*, 2439. https://doi.org/10.3390/cells10092439.

118. Kim, D., Langmead, B., and Salzberg, S.L. (2015). HISAT: a fast spliced aligner with low memory requirements. Nat. Methods *12*, 357–360. https://doi.org/10.1038/nmeth.3317.

119. Liao, Y., Smyth, G.K., and Shi, W. (2014). featureCounts: an efficient general purpose program for assigning sequence reads to genomic features. Bioinformatics *30*, 923–930. https://doi.org/10.1093/bioinformatics/btt656.

120. Robinson, M.D., McCarthy, D.J., and Smyth, G.K. (2010). edgeR: a Bioconductor package for differential expression analysis of digital gene expression data. Bioinformatics *26*, 139–140. https://doi.org/10.1093/bioinformatics/btp616.

121. Krueger, F., and Andrews, S.R. (2011). Bismark: a flexible aligner and methylation caller for Bisulfite-Seq applications. Bioinformatics *27*, 1571–1572. https://doi.org/10.1093/bioinformatics/btr167.

122. Du, P., Zhang, X., Huang, C.-C., Jafari, N., Kibbe, W.A., Hou, L., and Lin, S.M. (2010). Comparison of Beta-value and M-value methods for quantifying methylation levels by microarray analysis. BMC Bioinf. *11*, 587. https://doi.org/10.1186/1471-2105-11-587.

123. Strawn, M., and Behura, S.K. (2022). Epigenetic regulation of fetal brain development in pig. Gene *844*, 146823. https://doi.org/10.1016/j.gene.2022.146823.

124. Marsh, B., and Blelloch, R. (2020). Single nuclei RNA-seq of mouse placental labyrinth development. Elife *9*, e60266. https://doi.org/10.7554/eLife.60266.

125. Dobin, A., Davis, C.A., Schlesinger, F., Drenkow, J., Zaleski, C., Jha, S., Batut, P., Chaisson, M., and Gingeras, T.R. (2013). STAR: ultrafast universal RNA-seq aligner. Bioinformatics *29*, 15–21. https://doi.org/10.1093/bioinformatics/bts635.

126. Cieslak, M.C., Castelfranco, A.M., Roncalli, V., Lenz, P.H., and Hartline, D.K. (2020). t-Distributed Stochastic Neighbor Embedding (t-SNE): A tool for eco-physiological transcriptomic analysis. Mar. Genomics *51*, 100723. https://doi.org/10.1016/j.margen.2019.100723.

127. Hammond, T.R., Dufort, C., Dissing-Olesen, L., Giera, S., Young, A., Wysoker, A., Walker, A.J., Gergits, F., Segel, M., Nemesh, J., et al. (2019). Single-Cell RNA Sequencing of Microglia throughout the Mouse Lifespan and in the Injured Brain Reveals Complex Cell-State Changes. Immunity *50*, 253–271.e6. https://doi.org/10.1016/j.immuni.2018.11.004.

128. Luo, C., Keown, C.L., Kurihara, L., Zhou, J., He, Y., Li, J., Castanon, R., Lucero, J., Nery, J.R., Sandoval, J.P., et al. (2017). Single Cell Methylomes Identify Neuronal Subtypes and Regulatory Elements in Mammalian Cortex. Science *357*, 600–604. https://doi.org/10.1126/science.aan3351.

129. Hu, G., Li, J., and Wang, G.-Z. (2020). Significant Evolutionary Constraints on Neuron Cells Revealed by Single-Cell Transcriptomics. Genome Biol. Evol. *12*, 300–308. https://doi.org/10.1093/gbe/evaa054.

130. Jiang, J., Wang, C., Qi, R., Fu, H., and Ma, Q. (2020). scREAD: A Single-Cell RNA-Seq Database for Alzheimer's Disease. iScience *23*, 101769. https://doi.org/10.1016/j.isci.2020.101769.

131. Livak, K.J., and Schmittgen, T.D. (2001). Analysis of relative gene expression data using real-time quantitative PCR and the 2(-Delta Delta C(T)) Method. Methods *25*, 402–408. https://doi.org/10.1006/meth.2001.1262.

132. Bhattacharya, A., and De, R.K. (2009). Bi-correlation clustering algorithm for determining a set of co-regulated genes. Bioinformatics *25*, 2795–2801. https://doi.org/10.1093/bioinformatics/btp526.

133. Steuer, R., Kurths, J., Daub, C.O., Weise, J., and Selbig, J. (2002). The mutual information: detecting and evaluating dependencies between variables. Bioinformatics *18*, S231–S240. https://doi.org/10.1093/bioinformatics/18.suppl_2.s231.

134. Radovic, M., Ghalwash, M., Filipovic, N., and Obradovic, Z. (2017). Minimum redundancy maximum relevance feature selection approach for temporal gene expression data. BMC Bioinf. *18*, 9. https://doi.org/10.1186/s12859-016-1423-9.

135. Galili, T. (2015). dendextend: an R package for visualizing, adjusting and comparing trees of hierarchical clustering. Bioinformatics *31*, 3718–3720. https://doi.org/10.1093/bioinformatics/btv428.

STAR★METHODS

KEY RESOURCES TABLE

REAGENT or RESOURCE	SOURCE	IDENTIFIER
Deposited data		
Raw and processed data: snRNA-seq	This paper	GEO: GSE214759
Raw and processed data: bulk RNA-seq (wildtype and knockout fetal brain)	This paper	GEO: GSE215139
Raw and processed data: bulk RNA-seq (wildtype aging brain)	Islam et al.[5]	GEO: GSE215138
Raw and processed data: bulk RNA-seq (knockout aging brain)	This paper	GEO: GSE215139
Metabolomics	This paper	Table S1
DNA methylation	This paper	Table S7
Experimental models: Organisms/strains		
Mice: C57BL6/J (Strain #:000664)	The Jackson Laboratory	RRID:IMSR_JAX:000664
Mice: B6.Cg-Cav1^{tm1Mls}/J (Strain #:007083)	The Jackson Laboratory	RRID:IMSR_JAX:007083
Oligonucleotides		
List of primers for qRT-PCR data validation, see Table S14	This paper	N/A

RESOURCE AVAILABILITY

Lead contact

Further information and requests for resources and reagents should be directed to and will be fulfilled by the corresponding author, Susanta K. Behura (behuras@missouri.edu).

Materials availability

This study didn't create new mouse model to share. The mice used in this study are available for purchase from The Jackson Laboratory. Strain numbers are listed in the key resources table.

Data and code availability

- The snRNA-seq, and bulk RNA-seq data (both raw and processed) have been deposited in the Gene Expression Omnibus (GEO) database and are publicly available as of the date of publication. The accession number for snRNA-seq data is GEO: GSE214759. The accession numbers for bulk RNA-seq are GEO: GSE215138 and GEO: GSE215139. The metabolomics and methylation data are provided in the supplemental files within this study. File numbers are listed in the key resources table.
- This paper does not report original code.
- Any additional information required to reanalyze the data reported in this paper is available from the lead contact upon request.

EXPERIMENTAL MODEL AND STUDY PARTICIPANT DETAILS

Mice

The WT (C57BL/6J) and *Cav1*-null mice were obtained from Jackson Laboratory (stock numbers: 000664 and 007083 respectively). Adult females were mated with fertile males to induce pregnancy. The start of pregnancy (day 1) was considered when a vaginal plug was observed. The pregnant mice were euthanized on GD15, and the whole fetal brain was collected.[56] The samples were washed in sterile PBS and snap frozen in liquid nitrogen. Additionally, *Cav1*-null mice were aged to 70 weeks to collect aging brain. All animal procedures were approved by the Institutional Animal Care and Use Committee of the University of Missouri, and were conducted according to the Guide for the Care and Use of Laboratory Animals (National Institutes of Health, Bethesda, MD, USA).

METHOD DETAILS

Metabolomics analysis of fetal brain

The WT and *Cav1*-null fetal brain samples, in three replicates, were processed at the University of Missouri Metabolomics Center for untargeted metabolomics profiling of by gas chromatography–mass spectrometry (GC-MS). An Agilent 6890 GC coupled to a 5973N MSD mass spectrometer was used for GC-MS analysis. The replicate sample represented the whole brain from individual male and female fetuses. Using pestle and mortar, each sample was homogenized dry. 1 mg of the homogenate was mixed with 0.5mL of chloroform containing 10.0 μg/mL docosanol (as a non-polar internal standard) by vortexing for 1 minute. The mixture was then incubated at 50°C for 45 minutes in an oven with

periodical shaking. The samples were equilibrated at room temperature and then added with 0.5ml of water containing 25 μg/mL ribitol (as a polar internal standard) and vortexing for 1 minute. The mixture was incubated at 50°C for 45 minutes. The samples, after allowing to equilibrate to room temperature, were centrifuged at 3000xg for 30 minutes at 4°C to separate the solution into two layers, and 1ml of each layer was transferred into 2.0mL auto-sampler vials using a syringe. The syringe was washed three times using chloroform (for organic layer) and methanol (for aqueous layer). The aqueous polar layer (upper layer) was dried in a rotary evaporator.

Derivatization of polar metabolites was performed by adding 40μL of freshly prepared methoxyamine solution followed by brief sonication and incubation at 50°C for 1h. The samples were allowed to equilibrate at room temperature, and then added with 40μL N-Trimethylsilyl-N-methyl trifluoroacetamide (MSTFA) and 1% trimethylchlorosilane (TMCS) followed by incubation for 1h at 50°C. After the samples were cooled down to room temperature, 1.0 μL of the solution was injected at 15:1 split ratio onto a HP 6890N GC equipped with a 60M DB-5-MS column coupled to a HP 5973N MS. The injection port and transfer arm were held at 280°C. Separation was achieved with a temperature program of 80°C for 2 min, then ramped at 5°C per min to 315°C and held for 12 min at a constant flow of 1.0 mL/min. The MS source was held at 250°C, and scanned from m/z 50-650. Derivatization of polar metabolites was performed by resuspending the non-polar layer of each sample in 0.4 ml of chloroform and hydrolyzed by adding 0.5 mL of 1.25 M HCl in MeOH. After evaporating the solvents, the samples were re-suspended in 35 μL pyridine, briefly sonicated, and incubated at 50°C until residue was dissolved. Then 30 μL of MSTFA+ 1% TMCS were added, and the mixture was incubated 1hr at 50°C. After allowing the samples to equilibrate to room temperature, they were transferred to autosample vial with a 200 μL glass insert using glass pipette and analyzed using an Agilent 6890 GC coupled to 5973 MSD scanning from m/z 50-650. 1.0 μL of the solution were injected at 1:1 split ratio. The injection port and transfer arm were held at 280°C, separation was achieved with a temperature program of 80°C, for 2 min, then ramped at 5°C/min to 315°C and held for 12 min at a constant flow of 1.0 mL/min. The spectral analysis was performed by the AMDIS (Automated Mass Spectral Deconvolution and Identification System), and metabolites were identified using a commercial NIST17 mass spectral library. The abundance of the identified metabolites was determined by the Metabolomics Ion-Based Data Extraction Algorithm (MET-IDEA).[115]

Bulk RNA-seq analysis

Total RNA was isolated from GD15 fetal brain of WT and *Cav1*-null mice as well as from week 70 old *Cav1*-null mice using an AllPrep DNA/RNA Mini Kit (Qiagen, Cat No./ID: 80204) following the manufacturer's instruction. Samples from six female fetuses, three from WT and three *Cav1*-null mice, were used for RNA isolation. The RNA-seq data of week 70 WT mice brain was used from our earlier study[5] (Accession # GEO: GSE215138). For RNA extraction, samples were homogenized with 500 ul RLT buffer (Qiagen, Cat No./ID: 79216) supplemented with 5μl of 2-mercaptoethanol. The homogenate was transferred to a fresh tube and centrifuged for 1 minute at ≥ 8000 x g. From the supernatant, 750μl was transferred to a fresh tube and mixed with 1 volume 70% ethanol to precipitate RNA. RNA was eluted in 30μl nuclease-free water twice to a total volume of 60μl. Concentration of RNA was determined using a Nanodrop 1000 spectrophotometer (Thermo Fisher Scientific). RNA integrity was determined using Agilent 2100. The quality-checked RNA was used for preparation of libraries followed by library sequencing (RNA-seq) by the Novogene Cooperation Inc, Sacramento, CA. Each library was sequenced to 20 million paired end reads of 150 bases using a NovaSeq sequencer. RNA-seq data analysis was performed as described earlier.[116,117] Briefly, the quality of raw sequences was checked by *FastQC* followed by trimming the adaptors from the sequence reads by *cutadapt*. The *trimmomatic* tool was used to perform base quality trimming (Phred score >30) by sliding window scan (4 nucleotides). The quality reads were then mapped to the mouse reference genome GRCm39 using *Hisat2* aligner.[118] Read counting from the alignment data was performed by *FeatureCounts*.[119] The feature count data was then analyzed by *edgeR*[120] to determine significance of differential expression of genes in *Cav1*-null compared to WT brain.

DNA methylation analysis

DNA methylation of WT and *Cav1*-null fetal brain was profiled for the 2,045 CpG sites associated with mouse epigenetic clock.[5,57] Methylation profiling was performed by Zymo Research, Irvine, CA.[5] Briefly, genomic DNA from frozen brain samples were purified using Quick-DNATM Miniprep Plus kit (Cat. No. D4068). Bisulfite conversion was performed using the EZ DNA Methylation-Lightning TM Kit (Cat. No. D5030) followed by enrichment for target loci, and sequencing on an Illumina® HiSeq instrument. Sequence analysis was performed using *Bismark*[121] to extract methylation sites and beta-values[122] of methylation level for each site. Methylation data was analyzed in *R*.[5,123]

Single-nuclei RNA-seq

Single-nuclei RNA sequencing (snRNA-seq)[58,124] was performed to profile gene expression of single cells of female fetal brain (GD15) from WT and *Cav1*-null mice. Single nuclei were isolated using Pure Prep Nuclei Isolation kit (Product No. NUC-201, Sigma, St. Louis, MO, USA) as per manufacturer's instructions with slight modifications as follows. The frozen brain samples after thawing were minced into small pieces on a chilled petri dish on ice and added with 2ml lysis buffer supplied in the kit. The lysis buffer was freshly prepared by adding 1M dithiothreitol (DTT) and 10% Triton X-100. Using a dounce homogenizer, the samples were homogenized till the solution looked evenly mixed, which generally required 15-20 dounces. A 70μm cell strainer was used to filter the nuclei from the lysed cells. The filtrate that contained nuclei was diluted by adding 3ml additional lysis buffer and layered over a freshly prepared 1.8M sucrose cushion solution. Samples were centrifuged at 30,000xg for 45 minutes at 4°C to pellet the nuclei. After removing the supernatant, the pellet that contained nuclei was suspended with 1 ml of ice-cold storage buffer from the kit, and then centrifuged at 500xg for 5 minutes at 4°C. The supernatant was carefully removed and the nuclei pellet was resuspended in 200ul of ice-cold storage buffer from the kit. The suspension was then loaded onto a 40μm cell

strainer to collect the filtrate that contained the purified nuclei. Counting of nuclei was performed using a Countess II FL Automated Cell Counter (ThermoFisher).

The freshly prepared nuclei were used to prepare sequencing libraries using 10X Genomics Chromium Single Cell 3' GEM, Library & Gel Bead Kit v3.1 at the University of Missouri Genomics Technology Core. The nuclei suspension, reverse transcription master mix, and partitioning oil were loaded on a Chromium Next GEM G chip. Post-chromium controller GEMs were transferred to a PCR strip tube and reverse transcription was performed on an Applied Biosystems Veriti thermal cycler at 53°C for 45 minutes. cDNA was amplified for 12 cycles and purified using Axygen AxyPrep MagPCR clean-up beads. cDNA fragmentation, end-repair, A-tailing, and ligation of sequencing adaptors were performed according to manufacturer's specifications. The libraries were quantified using a Qubit HS DNA kit. The fragment size was analyzed using an Agilent Fragment Analyzer system. Libraries were sequenced on an Illumina NovaSeq 6000 with a sequencing configuration of 28 base pair (bp) on first read and 98 bp on the second read. Each library was sequenced to a depth of 20,000 paired-end (single-indexing) reads per nucleus. The base call (BCL) files were processed by the *Cell Ranger* pipeline (v. 3.0.1) to generate the FASTQ files. The *STAR* aligner[125] was used to map the reads to the mouse reference genome GRCm39 to generate read count data of genes of single cells.

The read count data was processed by *Seurat*[59] to identify expression clusters, and assign the clusters to cell types. Briefly, WT and *Cav1-null* brain read count data were integrated based on integration anchors identified from the first 20 dimensions of data variation. The scaled-normalized integrated data was subjected to cluster identification by principal component analysis (PCA) and non-linear dimensional reduction by tSNE (t-distributed stochastic neighbor embedding).[126] The '*FindAllMarkers*' function of *Seurat* was used to identify marker genes of each cluster. The cell types of the predicted clusters were annotated based on marker genes of brain cells curated in *PanglaoDB*[60] and recently published single-cell RNA studies of brain.[127–130]

Data validation

To further validate gene expression data of RNA-seq, we performed qRT-PCR with a selected set (*Hspg2, Mmp9, Igf2, Eif3j1*, and *Hbb-bt*) of genes. The qRT-PCR assays[56] were performed as follows. Briefly, total RNA (500 ng) from the fetal (GD15) and aged brain (week 70) from WT and *Cav1*-null mice were reverse transcribed in 10 μl reaction volume by *RevertAid* reverse transcriptase and oligo $(dT)_{18}$ primer. Three replicates were used for each of the four groups. So, a total of 12 samples were used in the qRT-PCR analysis. The *RevertAid* First Strand cDNA Synthesis Kit (catalog # K1621, ThermoFisher Scientific) was used for cDNA synthesis as per manufacturer's instruction. The qRT-PCR assays were performed using SYBR™ Select Master Mix (catalog # 4472903, ThermoFisher Scientific, Waltham, MA) and gene-specific primers in 10ul reaction volume. The gene-specific primers were designed using *Primer3web* (version 4.1.0) tool and synthesized by Integrated DNA Technologies (IDT, Coralville, IA). The sequences of the forward and reverse primers for each gene are provided in Table S14. *Gapdh* was used as a reference gene. The *Gapdh* primers as well as positive RNA control used in the assay were supplied in the SYBR™ Select Master Mix kit. Along with positive control with the kit-supplied RNA, negative controls, one without enzyme and another without the test RNA, were included for each sample. The three replicates were run for each sample in a 384-well plate using the BioRad CFX384 Real-Time System. The thermocycle conditions were 50°C for 2 minutes (min) and 95°C for 2 min for hot start activation of enzyme followed by 40 cycles of 95°C for 15 seconds and 60°C for 1 min. Data analysis was performed using delta-delta cycle threshold method[131] to calculate relative expression of gene compared to the reference. Pearson correlation coefficient was used to assess similarity in expression changes between qRT-PCR and RNA-seq data for each of the test genes.

QUANTIFICATION AND STATISTICAL ANALYSIS

The integrative metabolomics and RNA-seq data analysis was performed by mapping the deregulated metabolites and genes to KEGG compound and gene databases respectively. We have illustrated the approach in Figure 2. The genes and metabolites that mapped to the same pathways were identified, and they were used to integrate the RNA-seq and the metabolomics data. The resulting combined dataset was then analyzed by applying two-dimensional clustering technique called as biclustering.[50,132] We used biclustering to determine data variation of both rows and columns which contrasts from one-dimensional clustering techniques in which ether rows or columns are analyzed. We applied mean squared residue method[50] to calculate variation score for each metabolite-gene pair using the equation

$$\frac{1}{\|I\|\|J\|}\sum_{i\in I,j\in J}\left(a_{ij}-a_{iJ}-a_{Ij}+a_{IJ}\right)^2$$

where aiJ is the mean of row i, aIj is the mean of column j, and aIJ is the overall mean of the rows and columns. The calculated scores were then evaluated relative to scaling and threshold parameters, known as alpha and delta respectively, in order to select subsets of rows and columns to identify the biclusters. This was performed using *R* package *Biclust* with delta=0.001 and alpha=1 in three steps. In the first step, the rows and columns were deleted if they had scores larger than alpha times the matrix score. In the second step, the rows and columns with largest scores were removed. In the third and final step, rows and columns were added until the desired scaling (specified by alpha) was reached.

Mutual information (MI) network analysis[53] was performed to infer crosstalk between genes and metabolites. MI is a measure of the information that is shared between two variables calculated from the joint and marginal probability of variation.[133] MIs were calculated in a pair-wise manner between metabolites and genes from the combined RNA-seq and metabolomics data. An weighted adjacency matrix

of the MI values was generated by Maximum Relevance Minimum Redundancy (MRMR) method.[134] The adjacency matrix defined the degree of inter-dependence among genes and metabolites. Network inference was then made using *R* package *minet*.[53]

Canonical correlation analysis (CCA)[51] was performed to assess co-variation between genes and metabolites in *Cav1*-null relative to WT brain. This was performed using the *R* package *CCA*.[5] The receptor and ligand genes[56,116] were identified from the database developed by Ramilowski et al.[55] Hierarchical cluster analysis was performed using the *R* package *Dendextend*.[135]